EFFECT OF COOLING RATE ON THE MECHANICAL PROPERTIES OF GLASS FIBER POLYPROPYLENE COMPOSITES

by

Mohammed S. Kabbani

A Thesis Presented to the Faculty of the
American University of Sharjah
College of Engineering
in Partial Fulfillment
of the Requirements
for the Degree of

Master of Science in
Mechanical Engineering

Sharjah, United Arab Emirates

January 2017

Approval Signatures

We, the undersigned, approve the Master's Thesis of Mohammed S. Kabbani.

Thesis Title: Effect of Cooling Rate on the Mechanical Properties of Glass Fiber Polypropylene Composites

Signature	Date of Signature (dd/mm/yyyy)
_____	_____
Dr. Hany El Kadi Professor, Department of Mechanical Engineering Thesis Advisor	
_____	_____
Dr. Basil Darras Associate professor, Department of Mechanical Engineering Thesis Committee Member	
_____	_____
Dr. Sami Tabsh Professor, Department of Civil Engineering Thesis Committee Member	
_____	_____
Dr. Mamoun Abdel Hafez Head, Department of Mechanical Engineering	
_____	_____
Dr. Mohamed El-Tarhuni Associate Dean, College of Engineering	
_____	_____
Dr. Richard Schoephoerster Dean, College of Engineering	
_____	_____
Dr. Khaled Assaleh Interim Vice Provost for Research and Graduate Studies	

Acknowledgments

I would like to express my gratitude to my supervisor professor and associate dean of engineering Dr. Hany El Kadi of the department of mechanical engineering at American University of Sharjah for the useful comments, remarks and engagement through the learning process of this master thesis. The door to Prof. El Kadi's office was always open whenever I ran into a trouble spot or had a question about my research. Furthermore I would also like to thank the members of my thesis committee for the excellent recommendations they provided during the proposal and the thesis defense. Also, I would like to thank my loved ones, who have supported me throughout entire process, both by keeping me harmonious and helping me putting pieces together. I will be grateful forever for your love.

Abstract

Composite materials have been widely used in the recent years in almost all of the industries specially the high technology industries. Properties of the thermoplastic-based composites are affected by their processing conditions. Therefore, understanding of the behavior of these materials under different processing conditions is of most importance. Artificial Neural Networks (ANN) have recently been successfully used in the study of composite materials. This study aims to predict the mechanical properties of unidirectional glassfiber polypropylene composite materials processed under different cooling rates as a function of the fiber orientation angle using ANN. Composite specimens with five different fiber orientation angles were manufactured under different cooling rates using a compression molding press. These specimens were tested under static tensile stress to extract some of the mechanical properties such as the ultimate strength and strain and the modulus of elasticity. The stress-strain data of all but one of the conditions (cooling rate and fiber orientation) were used to train the ANN and predict the stress-strain behavior for the remaining condition. The influence of ANN parameters such as type of ANN, number of hidden layers, number of neurons per hidden layer, and number of iteration of the network training on the prediction accuracy has been investigated. The best predictions were obtained by using a multilayer perceptron (MLPs) with two hidden layers and 50 neurons in each, both hidden layers were trained using RProp learning rule for 1000 epochs. For all of the cases investigated, the modulus of elasticity was predicted with a minimum accuracy of 97% while the ultimate strain was predicted, in most cases, with a minimum accuracy of 90%. These predictions indicate that ANN can be successfully used to predict the mechanical properties of unidirectional composites manufactured under different cooling rates.

Search Terms: Unidirectional Composites, Glass Fiber Polypropylene, ANN, Processing Conditions, Cooling Rate.

Table of Contents

List of Figures

List of Tables

Nomenclature

ANN: Artificial Neural Network

CF: Carbon Fiber

CMC: Ceramic matrix composite

E: Modulus of elasticity

GF: Glass Fiber

MMC: Metal matrix composite

NMSE: Normalized mean square error

PEEK: Polyetheretherketon

PMC: Polymer matrix composite

PP: Polypropylene

PPS: Polypheneylene sulfide

PVDF: Polyvinylidene difluoride

r: Correlation coefficient

σ: Normal stress

ε: Normal strain

δ: extension

Chapter 1. Introduction

Composites were found in nature much before their discovery by mankind; the wood in the trees is considered to be a composite material. The development of artificial composites materials started coincidentally in 1930 when an engineer became intrigued by a fiber that was formed during the process of applying lettering to a glass milk bottle [1]. In 1935, some fiberglass companies such as Owens Corning Fiberglass Company in the United States and Nitto Boseki Company in Japan were established. Since then, more composites materials have been developed and improved in a rapid manner. Nowadays, we can see the wide use of composite materials in a big range of light and the heavy industries starting with the daily life use equipment, automobiles, rockets and space shuttles.

Due to the vital role that composites materials have played in recent years, many kinds of composites materials have been developed in order to satisfy the market needs. This resulted in a wide domain of composites that differ in the fiber, the matrix, and the process of formation. One of the main classifications of composites is by the type of matrix; metal (MMC), ceramic (CMC), or polymer (PMC). In this study, only polymeric-based composites will be considered [2].

1.1. Significance of the Research

The significance of this research is to use the Artificial Neural Networks (ANN) approach to predict the mechanical properties of unidirectional glass fiber polypropylene composite materials manufactured under different cooling rates. To the author's knowledge, such a use has not been attempted before. Experimental results obtained by testing a number of glassfiber polypropylene specimens processed at different cooling rates will be used as training data. This exercise will provide a solid base that will help predicting the mechanical properties of the same material processed using different cooling conditions. This will minimize the need to test the material under a larger number of processing conditions in order to determine its mechanical properties.

1.2. Aims of the Study

The main objective of this work is to use the static tensile behavior of a unidirectional glassfiber polypropylene composite material prepared using a number

of cooling rates to predict the material behavior under other cooling rates. This will help saving a lot of money and time, by performing a few tests (20) instead of performing hundreds of experiments to cover the whole range of the process conditions that can affect the material properties.

1.3. Methodology

In order to achieve the objectives and aims mentioned above, the work carried out through this study was divided into two main parts. The first part is to manufacture a number of unidirectional glassfiber polypropylene with 5 different fiber orientation angles (0, 30, 45, 60, and 90 degrees) under different cooling rates (slow, medium, and fast). A Wabash compression press will be used to manufacture the required specimens. Specimens of various fiber orientation angles manufactured under the above-mentioned cooling rates were tested under tension to obtain the mechanical properties from the stress-strain curves that will be generated for all conditions. Analyzing the result obtained will help determining the effect of cooling rate on the mechanical properties of the material. The second part of this study was to develop an Artificial Neural Network (ANN) model that can accurately predict the mechanical properties of glassfiber polypropylene composites processed under various cooling rates. Training the network using experimental data obtained for a variety of fiber orientations and cooling rates, the ANN would be able to predict the material behavior under other conditions not used during the training.

1.4. Thesis Organization

The rest of the thesis is organized as follows: Chapter 2 presents a literature review relating to the effect of process conditions on mechanical properties of composites as well as the basics of ANN and their previous use in the field of composites. Chapter 3 covers the experimental investigation including the stress strain curves obtained for the various fiber orientation angles and cooling rates considered. Chapter 4 includes the predictions obtained using ANN for the various cases considered as well as the effect of the various ANN properties on the prediction. Finally the conclusion and recommendations for future work are presented in Chapter 5.

Chapter 2. Literature Review

This chapter gives an introduction on composite materials, their types, process and the effect of processing conditions on their mechanical properties. The chapter also introduces ANN with applications related to composite materials.

2.1. Thermoplastic vs. Thermoset Polymeric Composites

Polymeric composites can be categorized based on the type of polymeric matrix as the thermoplastic-based and thermoset-based composites. Thermoset-based composites were initially used in many industries especially in the aerospace applications, but due to the poor resistance to creep of the thermosets at high temperature the focus has shifted to thermoplastic-based composites [3]. The choice of each type depends on the application, since each type exhibits specific advantages and disadvantages in terms of processability and service performance. Table 1 shows process characteristics for both thermoplastic and thermoset matrices.

Table 1 Characteristics for both thermoplastic and thermoset matrices [4]

Property	Thermoset	Thermoplastic
Modulus of elasticity	High	Low
Service temperature	High	Low
Toughness	Low	High
Viscosity	Low	High
Processing temperature	Low	High
Relaxation time	Long	Short
Conversion costs	High	Low
Recyclability	Limited	Good

The main attraction to the thermoplastic-based composites is the ability for recycling of the waste parts, making them reliable from the economic and environmental point of view. Additional advantages of the thermoplastic-based composites are easy formability and high speed fabrication. Also, using thermoplastic-based composites can offer certain mechanical properties that are better than the thermoset-based composites adding to their advantages [5].

Many types of thermoplastic polymeric resin matrices such as polypropylene (PP), polyethylene (PE), Nylon 11 (Rilsan), polyvinylidene difluoride (PVDF), polypheneylene sulfide (PPS) and polyetheretherketone (PEEK) have been used in composites. For the purpose of this study, only polypropylene will be in consideration because of its low cost, low density, and excellent balance of properties. In addition polypropylene possesses high flexural strength because of its semi-crystalline nature and has good chemical resistance over a wide range of bases and acids. Additionally polypropylene has been experimentally proven to have a good fatigue resistance, good resistance to electricity, and can be easily repairable [6].

Comparing the performance of thermoset and thermoplastic based composites, a study by Henaff-Gardin and Lafarie-Frenot [7] found that thermoplastic-based composites had better performance in terms of tensile loading than that of thermoset-based composites. Additionally Lafarie-Frenot and Touchard [8] have compared the two kinds of composites in terms of shear load resistance and found that at the beginning of the load both kinds behave similarly but after crack initiation the thermoplastic-based composite behave more plastically and delay the failure much more than the thermoset-based composites.

2.1.1. Process of thermoplastic-based composites. During the last decade, many new processing techniques have been developed for manufacturing thermoplastic-based composites. The type of processing methods used depends on the application conditions and the quality level of the desired final product. These methods include: hand lay-up, hot pressing, thermoforming, pultrusion, filament winding, or by using autoclave. Most of the mentioned methods require high temperature while processing for consolidation [9, 10].

2.1.2. Thermoplastic based composites process stages. The typical processing procedure for preimpregnated (prepreg) thermoplastic-based composites can be broken down into the following stages:

a) Heating
b) Consolidation
c) Cooling and solidification

During the first stage (heating), the composite temperature is raised to a level which corresponds to the melting temperature of the polymer. After the composite reaches the required temperature, then the consolidation pressure takes place. To ensure that all voids are removed from the material, the pressure and temperature levels must be held constant for a certain time, resulting into the compaction and solidification of the laminate. During the final stage, and after the composite is kept at the high pressure and temperature for a given time, the composite is cooled down. This can be done using different methods depending on the desired cooling rate. To avoid any warpage of the composite plate, the temperature needs to be decreased to a certain level before releasing the consolidation pressure [11]. Figure 1 shows the three processing stages and the pressure and temperature changes in each stage.

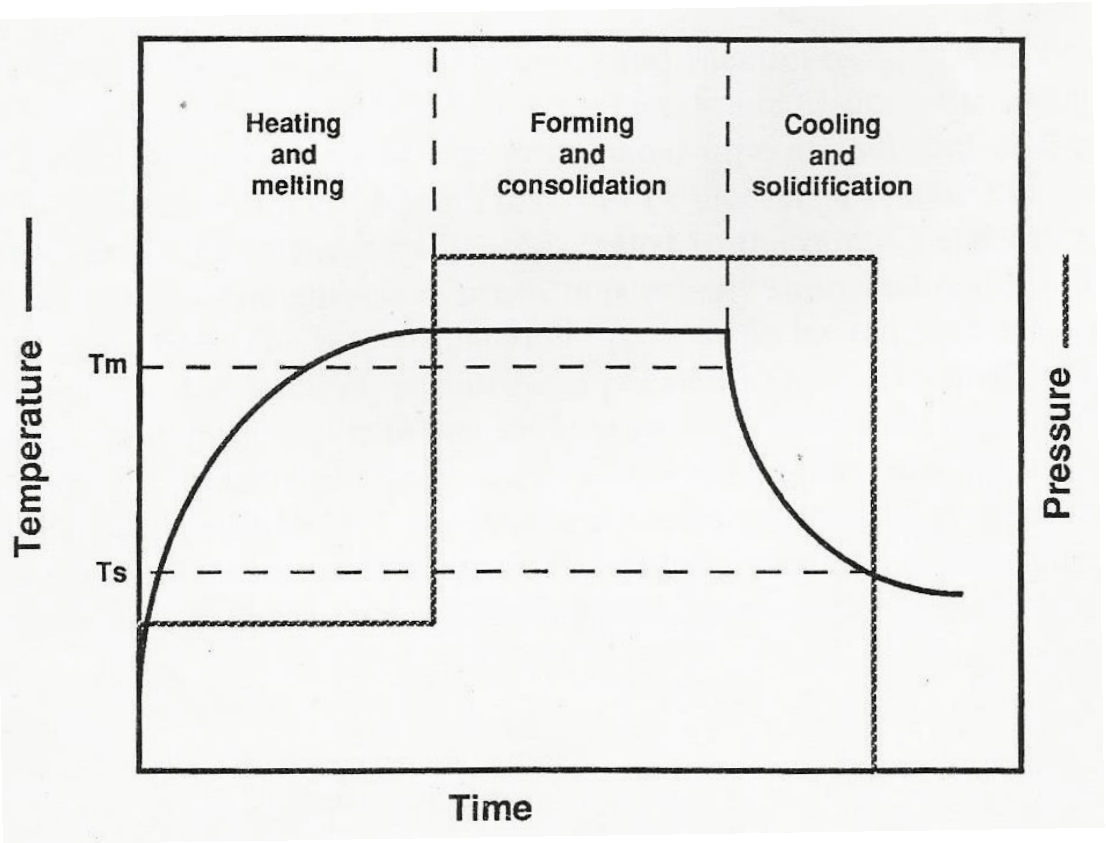

Figure 1 Processing stages of composites [11]

A preheating stage, where the composite piece is preheated in an oven before putting it in the mold, can be added to reduce time needed for consolidation as shown in Figure 2.

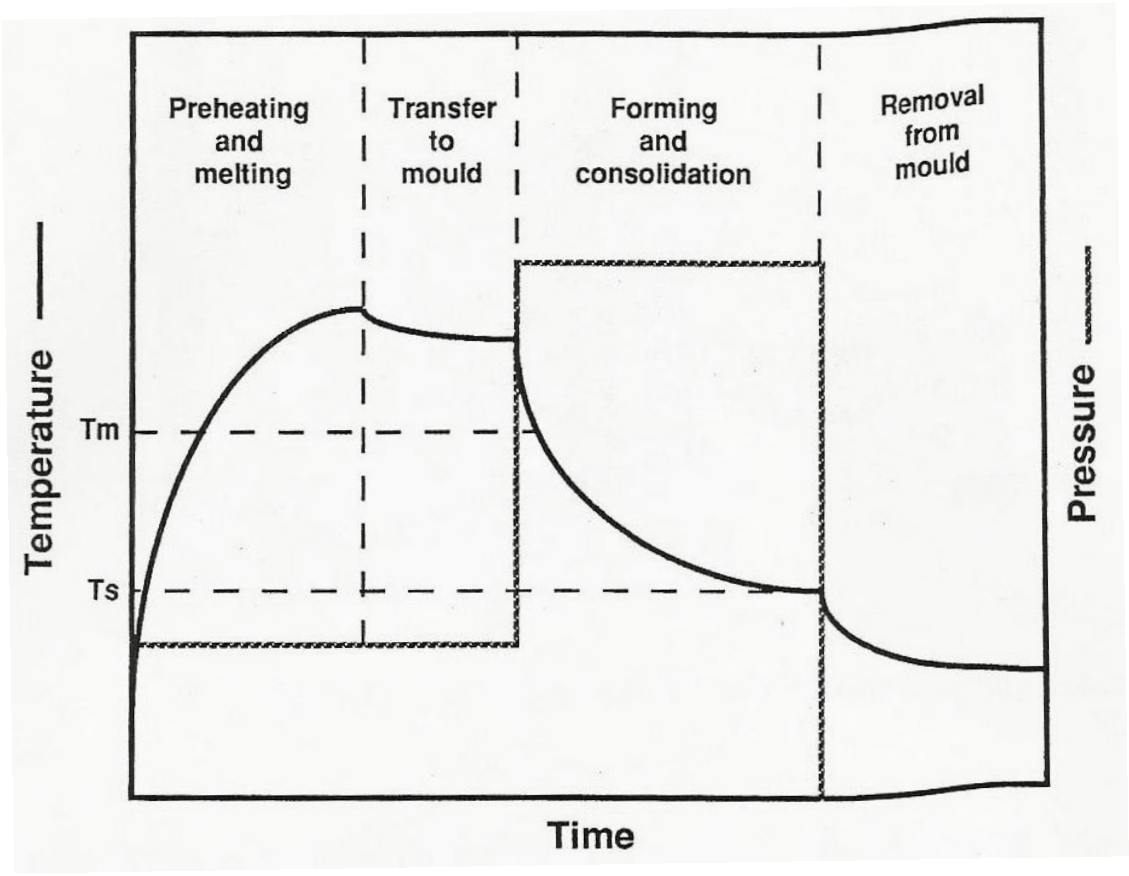

Figure 2 Changes in temperature and pressure in a processing cycle with preheating stage [11]

2.2. Effect of Process Conditions on the Mechanical Properties of Composites

The mechanical properties of a composite part or product can vary due to many reasons. These reasons could be determined before the process itself, such as the kind of fiber and matrix used to form the composite as well as the fiber orientation angle. The properties can also vary as a result of the process conditions used to prepare the final part. These conditions relate to cooling rate, curing temperature, curing pressure and the time of curing temperature. By controlling these parameters, different properties can result. Some of these process conditions have minor effects on the output while others (such as cooling rate) can significantly affect the mechanical properties of the composite produced [12, 13].

Before going in details about how process conditions affect the mechanical properties of composites, it is useful to describe those aforementioned conditions and provide a definition for each condition. Referring to Figure 1, the curing temperature and curing pressure are the temperature and pressure where consolidation takes place.

The curing temperature is always at the vicinity of the melting temperature of the polymer used. The time the composite is held at the curing temperature is called the curing temperature time. The cooling rate determines how fast the part will be cooled down from the curing temperature to room temperature. The cooling rate can be low by allowing the mold to cool down to room temperature on its own. A higher cooling rate can be obtained by cooling the mold using cold fluid (air, water…etc.). The cooling rate determines the degree of crystallinity of the polymeric composite (Figure 3) and is the most significant process parameter affecting the mechanical properties of the final part [14].

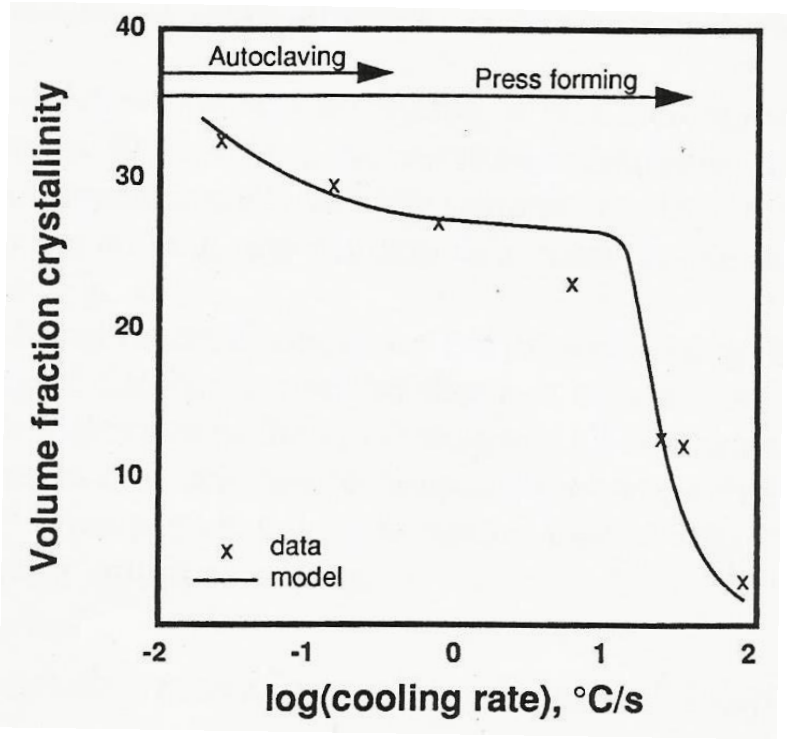

Figure 3 Relation between cooling rate and degree of crystallinity [14]

A number of studies have investigated the influence of process conditions on the mechanical properties of thermoplastic-based composites. Jar and Kausch [12] have studied the effect of curing temperature and cooling rate on the delamination resistance of CF/PEEK composites. They concluded that mode 1 and 2 delamination resistance decreases as curing temperature decreases and, as the curing temperature increases, better mechanical properties are achieved. They also concluded that cooling rate had significant effect on delamination resistance for cooling rates between 0.5 ˚C/min and 50 ˚C/min.

Another study on the effect of cooling rate was conducted by Davies et al. [13]. They studied the influence of cooling rate on long term mechanical properties, and found that, for a unidirectional specimens, the effect of cooling rate is minor but for multidirectional specimens lower cooling rate results in much better performance in terms of static and fatigue behavior. They also concluded that internal stresses in the material can be more harmful to the material performance when the material is subjected to high cooling rates.

The effect of cooling rate on the shear behavior of continuous glassfiber/impact polypropylene composites (GF-IPP) was investigated by Wafai et al. [15]. They found that increasing cooling rate improved the global mechanical properties, such as strength and strain at failure of both neat IPP and $[\pm 45]_s$ GS-IPP composites. They also found that the modified fiber matrix interface was able to maintain a strong bond at all investigated cooling rates as revealed by the SEM images of $[\pm 45]_s$ fracture surfaces. The concluded that by decreasing the cooling rate, the rate of stiffness degradation was increased and the effect of cooling rate on degradation occurred as a combination of mesoscale damage and the viscoelasticity of IPP. They also revealed that plasticity does not depend on the cooling rate once the viscoelasticity was removed.

Studies done by Tregub et al. [16, 17] on the effect of degree of crystallinity on the mechanical properties of CF/PEEK composites concluded that a high degree of crystallinity improves the mechanical properties of the composites. Deporter and Baird [18] investigated the influence of curing temperature, residence time at melt temperature, and cooling rate on the matrix morphology of semi crystalline materials such as PEEK and their composites. Tables 2 and 3 represent the results for two kinds of semicrystalline thermoplastic-based composites, where Ryton is a polyphenylenesulfide matrix composite reinforced by AS4 carbon fibers while XLC40-66 is an improved modification of Ryton. From the results, it clear that the degree of crystallinity increases with decreasing the cooling rates for both materials, and that the composites stiffness decreases with increasing the cooling rates, which means the higher degree of crystallinity leads to a stiffer composite.

Table 2 Effect of varying the cooling rate on the degree of crystallinity and flexural properties of Ryton [18]

Cooling rate (°C/min)	% Crystallinity	Strength (GPa)	Modulus of elasticity (GPa)
0.4	46 ± 2.3	1.9 ± 0.1	118 ± 2
4	30 ± 1.5	1.3 ± 0.1	107 ± 2
68	10 ± 0.5	0.9 ± 0.05	100 ± 4

Table 3 Effect of varying the cooling rate on the degree of crystallinity and flexural properties of XLC40-66 [18]

Cooling rate (°C/min)	% Crystallinity	Strength (GPa)	Modulus of elasticity (GPa)
0.4	46 ± 2.3	1.9 ± 0.2	132 ± 2
4	38 ± 1.9	2.0 ± 0.1	126 ± 3
68	28 ± 1.4	1.1 ± 0.1	115 ± 2

Davies et al. [19] investigated the effect of cooling rate after moulding on the fracture behavior of glassfiber polypropylene laminates. They found that the fracture behavior is strongly influenced by the cooling rate based on tested specimens been manufactured using the press method under various cooling rates (cooling rate range: 0.23 – 55 °C/min). They also concluded that the cooling rate affects the matrix structure as illustrated in Table 4.

Table 4 Effect of cooling rate on the matrix structure of glassfiber polypropylene composites [19]

Cooling rate (°C/min)	Degree of crystallinity (%)	Spherulitic structure
55	50 (±5)	Fine structure <10 µm, occasional larger spherulities.
2.6	61 (±5)	Large spherulities, 20 to 50 µm diameter, a few interspherulitic defects.
0.23	65 (±5)	Large spherulities, 20 to 50 µm diameter, many interspherulitic defects.

The influence of molding conditions and test temperatures on the interlaminar fracture toughness of the continuous glassfiber polypropylene composites has been studied by Perrin et al. [20]. In their study, specimens were manufactured under three molding conditions; normal molding condition (NM), the slowly cooled condition (SC) and the low temperature condition (LT) at two test temperatures (23 and -40 °C). The manufactured specimens were tested using fracture toughness test on double cantilever beam. Table 5 shows the results obtained from the fracture toughness test.

Table 5 Effect of molding condition and test temperature on the fracture toughness of CGF/PP composites [20]

Test temperature (°C)	Condition	$G_{IC,onset}$ (J/m^2)	$G_{IC,prop}$ (J/m^2)
23	NM	1270	2000
	SC	200	770
	LT	220	960
-40	NM	1060	1900
	SC	220	920
	LT	230	900

Another study addressing the effect of molding conditions on the interlaminate fatigue crack propagation of continuous glassfiber polypropylene composites was conducted by Bureau et al. [21]. They concluded that low cooling rates (below 1 °C/min) resulted in weaker interspherulitic changes which resulted in incomplete melting of the polypropylene matrix, and that microstructural changes lead to poor fatigue resistance. At higher cooling rates (above 10 °C/min) they obtained better fatigue resistance with crack propagation only occurring at the fiber-matrix interface. Figures 4, 5 and 6 show the micrographs obtained by SEM of the pre-polished surface of glassfiber polypropylene specimens processed under the different molding conditions. Table 5 shows the effect of molding conditions on the Young's modulus, flexural modulus, flexural strength and the interlaminate shear strength of the investigated material.

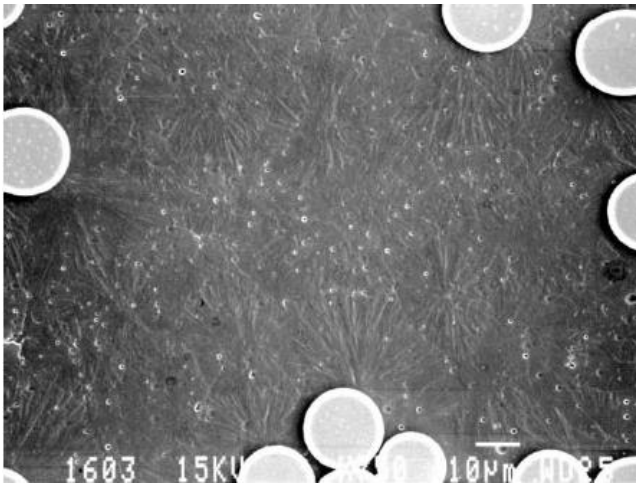

Figure 4 SEM micrograph of an etched pre-polished surface of the CGF/PP corresponding to NM condition [21]

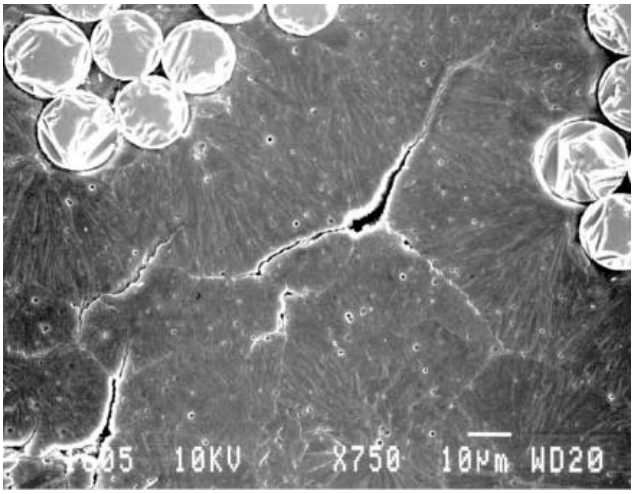

Figure 5 SEM micrograph of an etched pre-polished surface of the CGF/PP corresponding to SC condition [21]

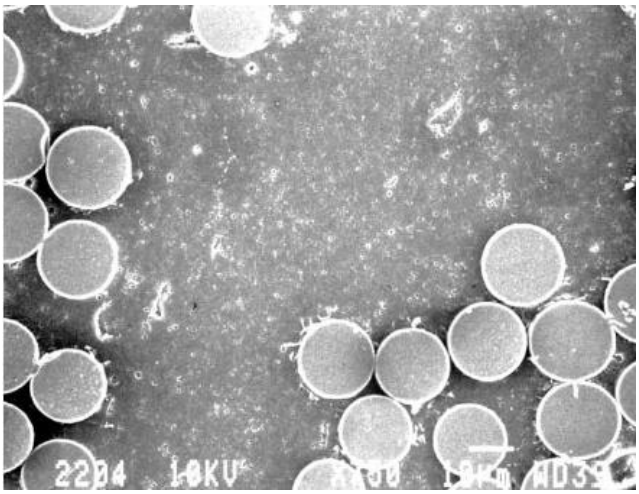

Figure 6 SEM micrograph of an etched pre-polished surface of the CGF/PP corresponding to LT condition [21]

Table 6 Effect of molding conditions on the mechanical properties of GF/PP composites [21]

Molding condition	Young's modulus (GPa)	Flexural modulus (GPa)	Flexural strength (MPa)	Interlaminate shear strength (MPa)
NM	25.7	24.6	470	51
SC	27.8	25.5	405	47
LT	29.1	25.6	395	15

A study done by Frihi et al. [22] investigated the analytical relationship for the crystallinity ratio of the PA66 matrix in glassfiber reinforced composites as a function of glass fiber content and cooling rate. In their study a good relationship was obtained and 95% correlation coefficient achieved. They concluded that both GF composition and processing condition strongly affect the crystallinity ratio of PA66/GF composites.

One of the latest studies on the effect of thermal history on composites by Regis et al. [23] investigated the effect of thermal history of the polymer on the crystallinity and mechanical properties of PEEK and CFR PEEK. They experienced an increase in crystallinity by lamellar thickening with annealing temperature through FTIR, WAXD and SAXS measurements. In addition, they found that samples with annealing temperature revealed a secondary melting peak in the DSC thermograms and indicating a growth of a population of thinner crystals upon annealing. They also concluded that annealing affected the mechanical properties of PEEK and CFR PEEK, indicating that crystallinity increase has strengthening effect in the presence of fiber reinforcement.

2.3. Artificial Neural Networks (ANN)

ANN can generally be defined as a structure composed of a number of interconnected units [24]. Each unit implements a local function and has an input/output characteristic. The output of each unit is determined by its input/output characteristic, its interconnection to other units and (possibly) external inputs, and its internal function. One or more forms of training used to develop the functionality of the ANN. The building block of the ANN is called artificial neuron [24]. The neuron has a set of weighted inputs. In order to understand how ANN operate, a brief introduction on the natural nervous system is required [25]; this is highlighted next.

2.3.1. Natural nervous system. Figure 7 shows an example of a typical neuronal cell from the spinal cord. These neuronal systems can decide the response of the body by gathering millions of bits of information from all over the body sensory receptors and integrate all this data to determine to correct response of the human body.

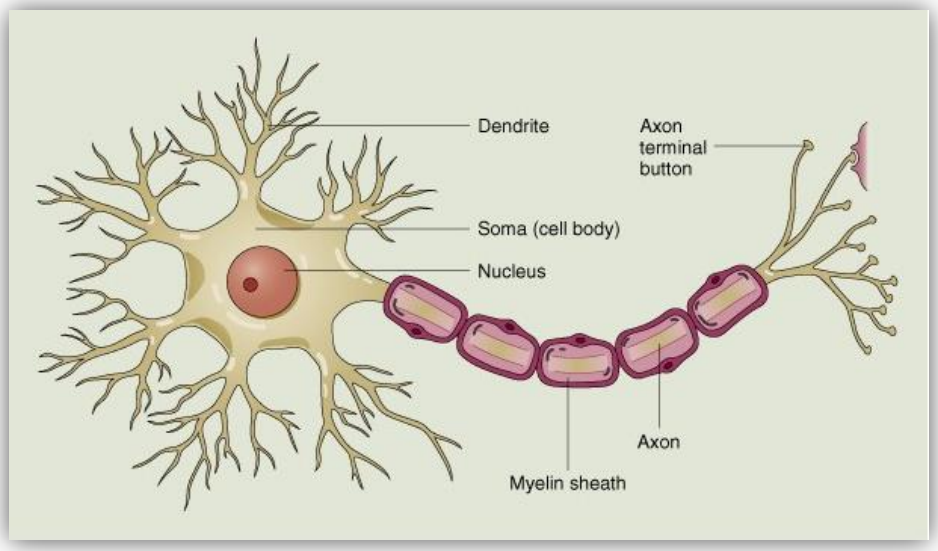

Figure 7 A typical neuronal cell from the spinal cord [26]

An adult human body contains more than 100 billion neurons. These neurons are connected with each other by junctions that allow the signal to be transmitted from neuron to another, the fibers from the transmitter neuron can be considered as the output and the fibers of the receiver neuron are the input as illustrated in Figure 8.

2.3.2. Artificial neural networks. After a brief description about the natural nervous system, it will be easier to understand how "artificial" neural networks work. The structure of ANN is similar to that of biological neurons, and consists of computational units called neurons that are arranged in layers connected to each other. The first layer consists of input units (neurons), and the last layer consists of output units. One or more layer called hidden layers can exist between the input and the output layers. These layers are called hidden layer because their input and output are hidden within the network. Increasing the number of hidden layers allows the network to extract higher-order statistics and get better prediction in case of large inputs. Figure 9 shows a general configuration example of ANN [24].

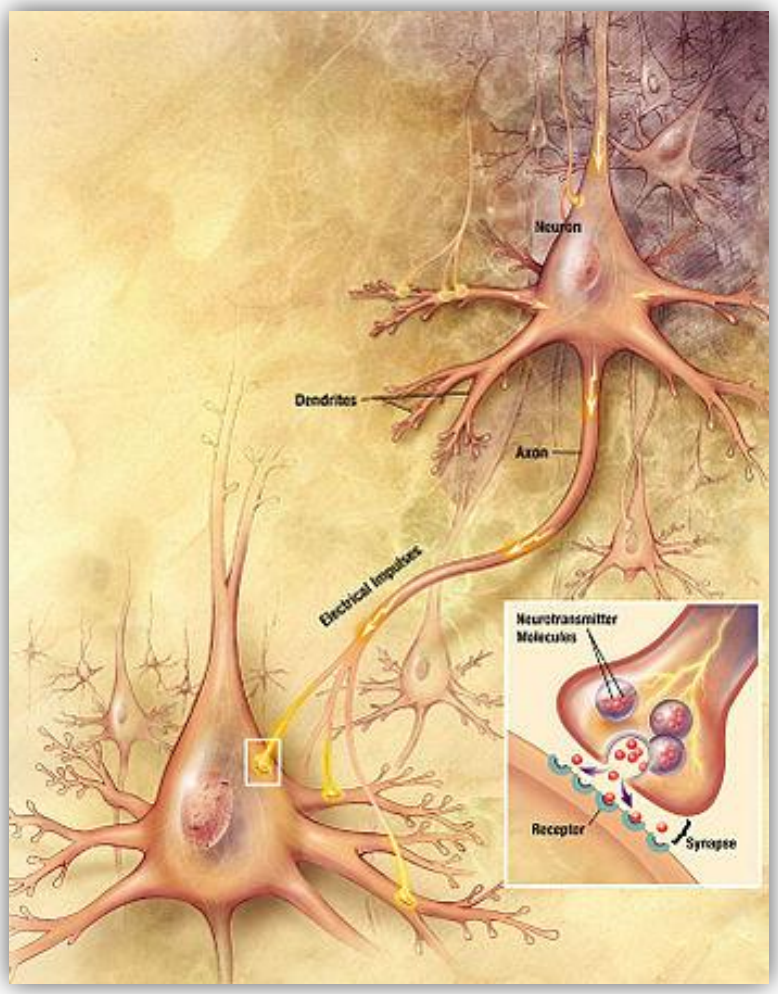

Figure 8 Example of biological Neurons junction [27]

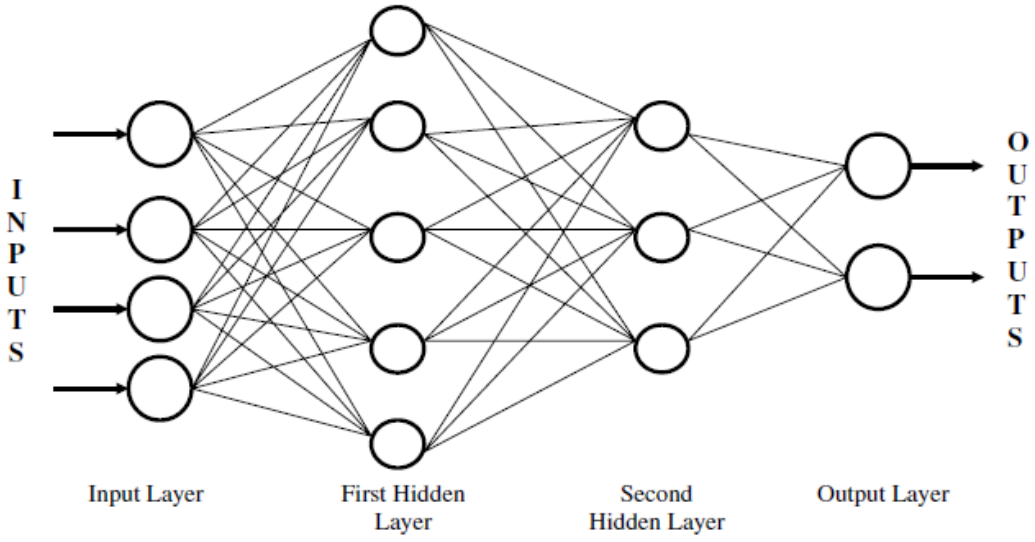

Figure 9 General configuration of ANN [23]

A more detailed general form of ANN is shown in Figure 10. The diagram shows 3 layers: the input layer with 4 inputs (X_1 to X_4), an output layer with 8 outputs (Y_1 to Y_8) and a single hidden layer. It is clear from the figure that every input is connected to all neurons in the following layer, using weight matrix (W). All inputs are weighted before being transmitted to the hidden layers. After the neurons receive all data from each input, they sum these inputs and generate an output; these outputs will be the inputs for a specified function f, the output of this function represented by the symbol y.

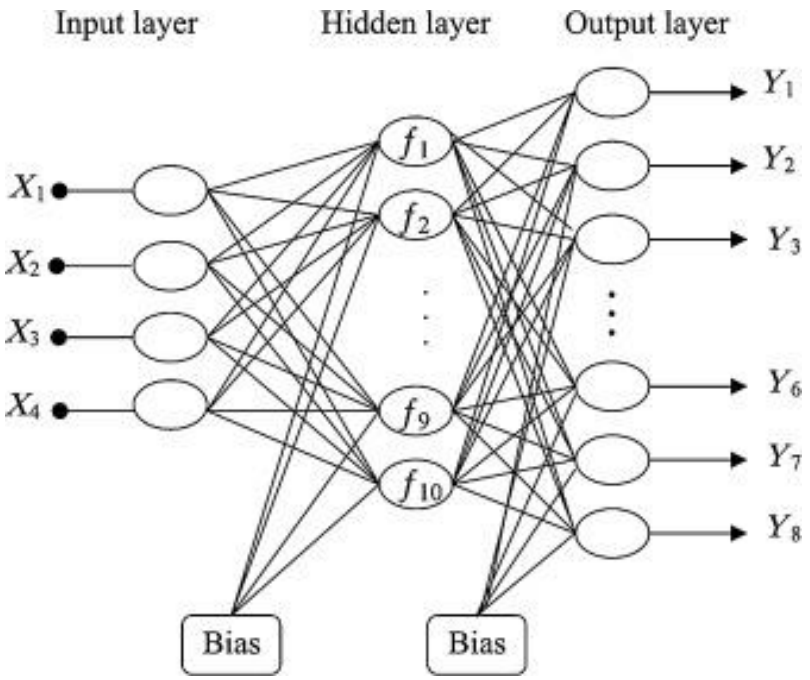

Figure 10 Detailed diagram of ANN [28]

A weight matrix is used because not all inputs have equal effect on the outputs, so each input need to be weighted with a specific percentage. The weight matrix can be written as follows:

$$W = \begin{bmatrix} W_{1,1} & \cdots & M_{1,n} \\ \vdots & \ddots & \vdots \\ W_{m,1} & \cdots & M_{m,n} \end{bmatrix} \quad (2.1)$$

Where,

n = number of inputs

m = number of neurons

The relation between the weighted inputs and the outputs y is given by:

$$y = f(W_p + b) \tag{2.2}$$

These relations can be also applied for a multilayer ANN that has more than one hidden layer.

2.3.3. Use of ANN to predict mechanical properties of composite materials. ANN has been recently used in many engineering applications. In this work, our interest is related to composite materials, and specifically to polymeric composites. Because of the large time and money consuming aspect of the composite material testing and the big domain of the type of test, type of composites, and the variation of the conditions and properties need to be investigated, the need of engineering software that can predict these kinds of tests accurately. The artificial neural networks (ANN) have the ability to learn by example and can deal with nonlinear modeling accurately without the need to deal with a very complicated analytical solution that has the same accuracy level [24].

Pidaparti and Palakal [29] addressed the modeling of composites using ANN in one of the first papers addressing this topic. They developed a back-propagation neural network to predict the non-linear stress–strain behavior of (±θ) graphite–epoxy laminates. In their investigation, an ANN with 3 inputs (fiber orientation, the initial stresses and incremental stresses) and 959 data points was used to predict the stress-strain behavior of the graphite/epoxy composites. The authors concluded that they can accurately predict the strain as an output. The four diagrams in Figure 11 show the good correlation between the experimental and predicted true stress-strain diagram for various strain rates.

Aymerich and Serra [30] used ANN to predict the fatigue strength of APC-2 composites. They used back propagation networks based on fiber orientation. They concluded that the training sets must cover the input varying range (fiber orientation angle) in order to obtain a good prediction. When only the upper or lower values were used as a training set, the predicted fatigue strength did not compare well with experimental data.

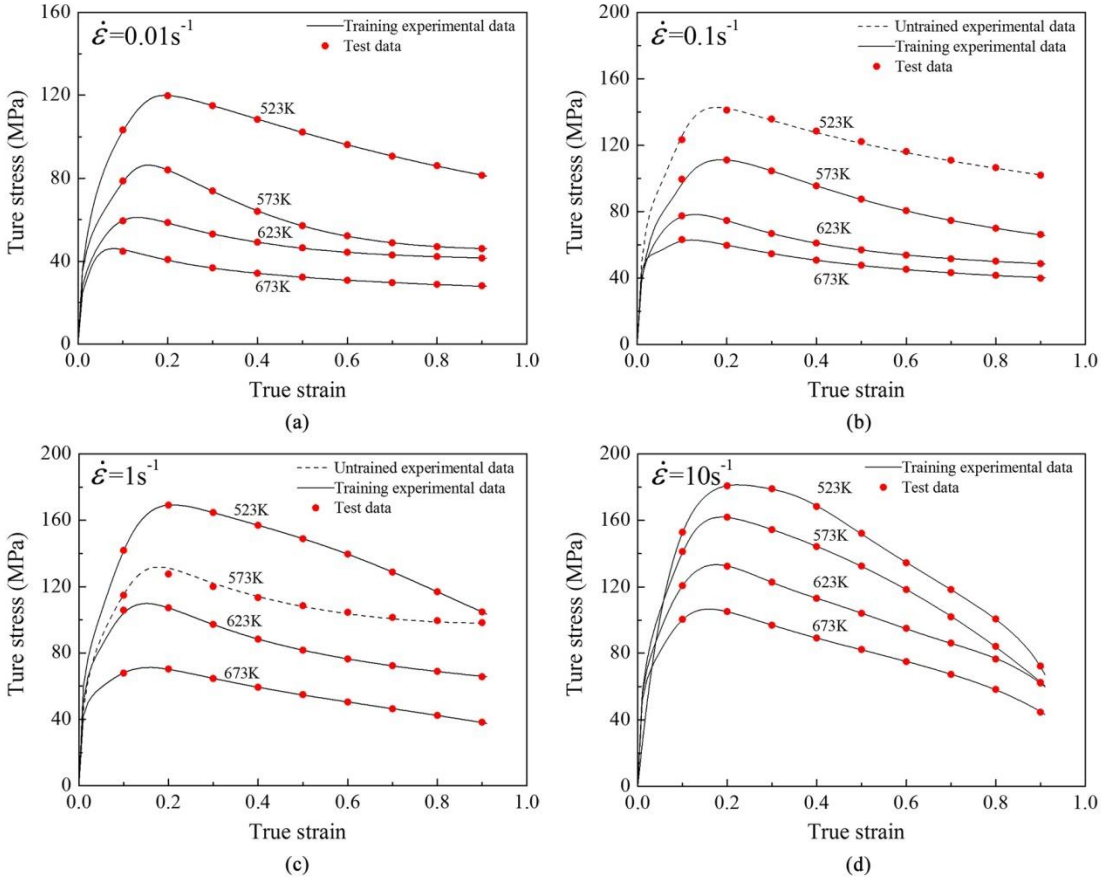

Figure 11 ANN predictions vs. experimental data of stress-strain behavior [29]

Some general results and suggestions for using ANN for composite material behavior prediction in general were recommended by number of authors, and it will be useful to cover some of them. Three studies by Al-Assaf and El Kadi [31] and El Kadi and Al-Assaf [32, 33] investigated the fatigue life prediction of fiberglass/epoxy laminae using ANN. In the first study [31], the feasibility of using ANN to predict fatigue failure was investigated. In a follow-up paper, El Kadi and Al-Assaf [32] compared the predictions they had obtained using the feedforward ANN with those obtained using a variety of other ANN structures. They concluded that the use of modular neural networks reduced the Normalized Mean Square Error (NMSE) from 14.2% to 5.7% and increased the Correlation Coefficient (r) from 92.6% to 97.3% (Table 7). The third study of the series, El Kadi and Al-Assaf [33] addressed reducing the complexity of the ANN by reducing the number of inputs.

Table 7 Comparison of NMSE and r for the various neural network structures [32]

	NMSE	r
FNN	0.14273	0.9260
MN	0.05668	0.9726
R BF	0.6600	0.4703
SOFM	0.0743	0.9624
PCAN	0.1402	0.9280

Zhang et al. and Jiang et al. [34, 35] suggested that an ANN is suitable for applications when the following conditions are satisfied: a large database is available, it is difficult to find an accurate solution to the problem by existing mathematical approaches, and the dataset is incomplete, noisy or complex.

Mishra et al. [36] developed an ANN model to predict the residual tensile strength of UD-GFRP composite laminates with drilled holes. The ANN model used in the study was a back propagation-artificial model consisting of three layers: input layer, output layer and a single hidden layer with 8 neurons. The input layer included three inputs: drill point geometry, spindle speed and feed rate, while the residual tensile strength was the lone variable included in the output layer. An adapting learning rate of 0.9 was used. The neural model was trained for 250 iterations. They found that the predicted values were in close agreement with the experimental values. They suggested that comprehensive experimental data including other drilling parameters that influence the drilling induced damage and affect the residual tensile strength of composite laminates will enhance the ANN model performance and could result in higher prediction accuracy.

One of the latest studies done by Shabani et al. [37] investigated the mechanical properties of A356 matrix reinforced with B_4C particulates experimentally, then modeled the mechanical properties including yield stress, ultimate strength, hardness and elongation percentage using a combination of artificial neural network and finite element techniques. The ANN used for the prediction purposes in their study was a fully developed feed forward back propagation model which contained 3 layers, the input layer including three input nodes: cooling rate, temperature gradient and volume

percentage of B_4C, the output layer including five output neurons: hardness, amount of porosities, UTS, yield stress, and fracture strain, and a single hidden layer. Sigmoid activation function was used to be the transfer function between all layers. They found that the predicted mechanical properties using ANN was in good agreement with experimental data. They concluded also that by using ANN model a considerable savings in terms of cost and time could by obtained.

Chapter 3. Experimental Investigation

3.1. Material and Specimens

The material used for this research was the fiberglass polypropylene composite material. A unidirectional prepreg tape produced by AtenPly was used in the processing of the specimens needed for testing. The material code provided is GPP45; the fibre material is E-Glass and the matrix is polypropylene. Table 8 and Table 9 show the physical properties and the mechanical properties respectively of the GPP45 tape as provided from the manufacturer specification sheet.

Table 8 Physical properties of AtenPly GPP45 tape [38]

Physical properties			
width	90 mm	**Density**	1.65
Thickness	0.25 mm	**Fibre content**	70 Wt %
Process Temperature	180 °C		45 V %

Table 9 Mechanical properties of AtenPly GPP45 tape [38]

Mechanical Properties	Units	Test Method	Unidirectional	0/90
Tensile Strength	MPa	ISO527		452
Tensile Modulus	GPa	ISO527		21.8
Tensile strain to break	%	ISO527		2.4
Flexural Strngth	MPa	ISO4125	464	323
Flexural Modulus	GPa	ISO4125	30	16
In-plane Shear Strength τ_{12}	MPa	ISO14129		28.4 (±45)

To ensure accurate and comparable results, the D 3039/D 3039M-08[1] standards developed by ASTM International Standards have been followed. This standard provides recommendations for sampling and testing specimens for the tensile test method of polymeric-based composites. Table 10 shows the tensile specimen geometry requirements as recommended by the ASTM standards.

[1] ASTM, Standard test method for tensile properties of polymer matrix composite materials

Table 10 Tensile specimen geometry requirements

Parameter	Requirement
Shape	constant rectangular cross-section
minimum length	gripping + 2 times width + gage length
specimen width	as needed
specimen width tolerance	±1 % of width
specimen thickness	as needed
specimen thickness tolerance	±4 % of thickness
specimen flatness	flat with light finger pressure

Based on Table 8, the final specimen dimensions were set to 250 mm in length, 20 mm in width, and 4 mm in thickness for fiber orientation angles 30, 45, 60 and 90, and 250 mm in length, 20 mm in width, and 2 mm in thickness for fiber orientation angle 0˚. The reduction of thickness of the 0˚ fiber orientation angle was necessary to avoid the possible slipping of the specimen within the machine grips during tests due to the high amount of load needed to be applied in case of thicker specimens. The picture aluminium mold used to manufacture the specimens is shown in Figure 12. The mold was manufactured using CNC cutting machine and consists of two parts, the base part where the prepreg laminas are placed (Figure 13) and the top part which will transfer the pressing load uniformly from the pressing machine to the prepreg laminas. The mold was designed with minimum clearance between the top and base parts to avoid resin leakage during processing.

Figure 12 Aluminum mold

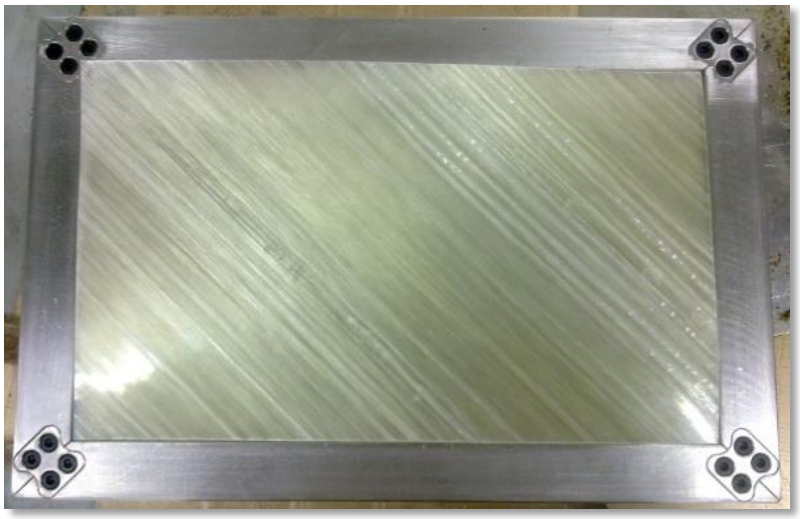

Figure 13 Aluminum mold with the prepreg laminas

3.2. Specimens Processing

3.2.1. Processing conditions. In order to study the effect of cooling rate on the static properties of the composites. All other processing conditions such as curing temperature, curing pressure and curing time were held constant throughout. These values were determined after a number of experiments were carried out. Table 11 shows the processing conditions that have been used to prepare the specimens.

Table 11 Processing conditions used in this study

Processing conditions	
Cooling rates	Slow / Medium / Fast
Curing temperature	180 ˚C
Curing pressure	8900 N
Curing time	5 min
No. of pre-preg laminas	10 layers (except for 0˚, 5 layers only)

The manufactured plates with required fiber orientation angles can be set by placing the fiber with the required angle in the mold. The cooling rates can be controlled using the options provided by the press machine as will be explained later. The curing temperature was set to 180 ^{o}C to insure that the resin will melt without getting burned as per the material supplier user guidance. The remaining parameters were set after some experiments were carried out to get the proper values that can suit the material under consideration.

3.2.2. Procedure. A programmable (Wabash) hydraulic press was used to carry out the processing of the specimens after the proper number of prepreg layers were placed in the mold at the required angle as shown in Figure 14.

Figure 14 Specimen processing procedure

Initial pressure of 2225 N (500 lbs) was applied while heating up the mold, the platens temperature was set to 200 ˚C to compensate for the heat loss between the press machine platens and the mold. To ensure reaching a temperature of 180 ˚C inside the mold, a thermocouple was place inside a 1 mm diameter hole on the side of the mold. After reaching the required curing temperature, the pressure was increased to reach the curing pressure of 8900 N (2000 lbs) and held for 5 minutes before turning off the heater. The mold was then cooled down using different methods to achieve the required three cooling rates. The slow cooling rate was obtained by stopping the heating process from the platens and letting the mold cool down on its own to room temperature. The medium cooling rate was obtained using the air cooling option provided by the press. Once the heating was turned off, air at room temperature (25 ^{o}C) was circulated through the platens of the press to accelerate the cooling of the mold. The fast cooling rate was obtained by selecting the combined air and water cooling option in the pressing machine. In this option, once the heater was turned off, the machine circulates both room temperature air and cold water at 15 ^{o}C through the platens. The thermal change during the curing cycle was monitored by a

very accurate data acquisition device connected to the thermocouple which was set to take reading every one second and up to two decimal places. Figure 15 shows the molding press in operation.

3.2.3. Curing cycle. The curing cycle which illustrates the relation between time and temperature change during the operation of the press machine was generated automatically from the software of the data acquisition in form of graphs. Figures 16, 17 and 18 show the different graphs for the three cooling rates considered.

Figure 15 Wabash compression press

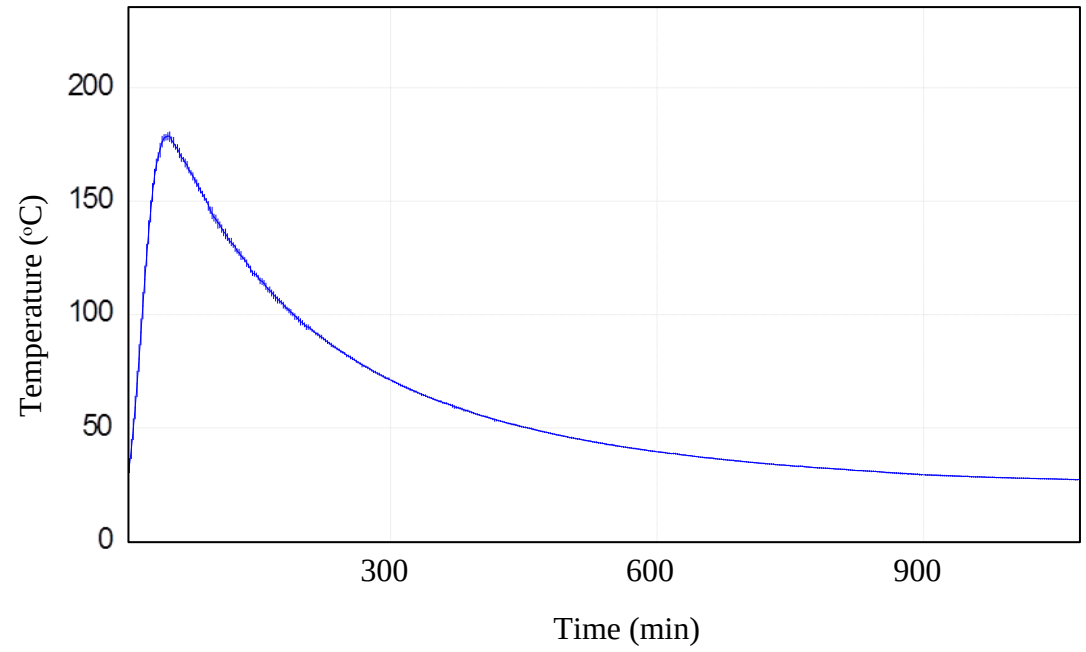

Figure 16 Slow cooling rate curing cycle

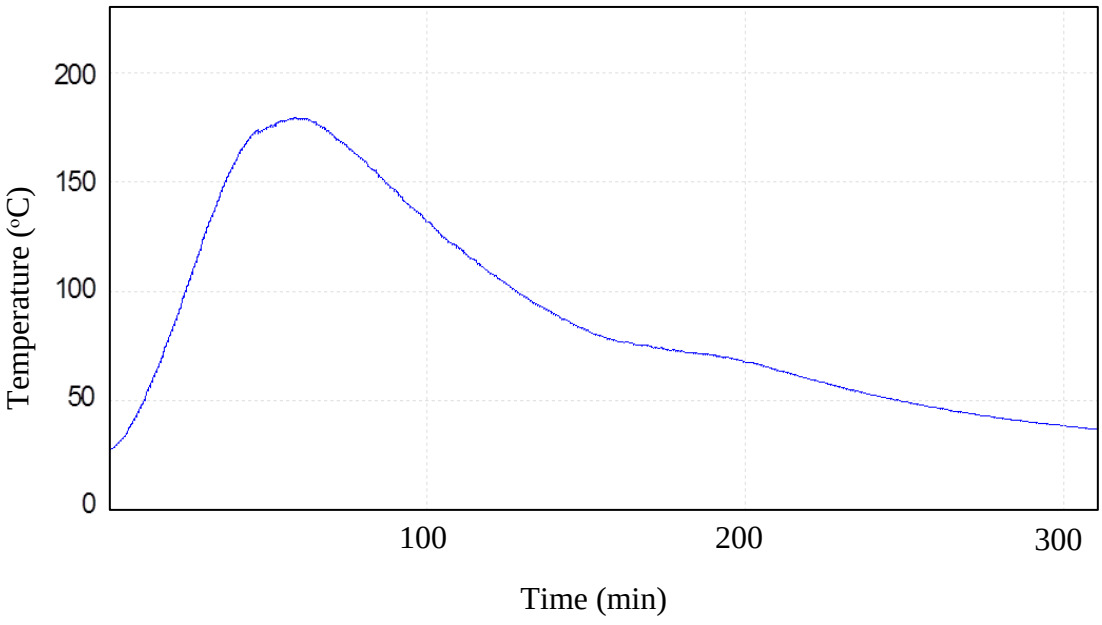

Figure 17 Medium cooling rate curing cycle

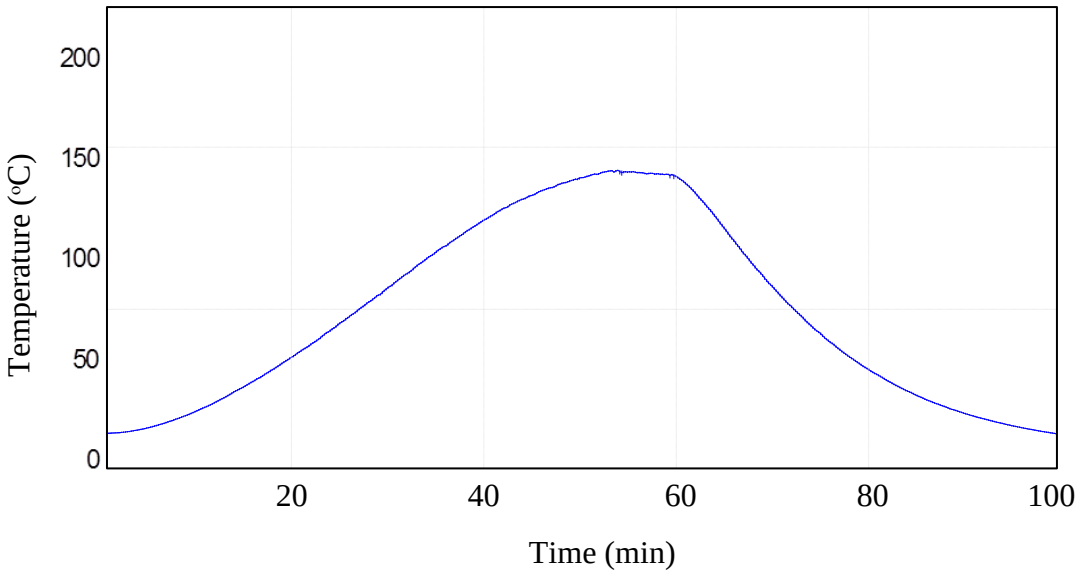

Figure 18 Fast cooling rate curing cycle

The value of the cooling rate was obtained by calculating the slope of the graph once the temperature starts decreasing as illustrated in Figure 19.

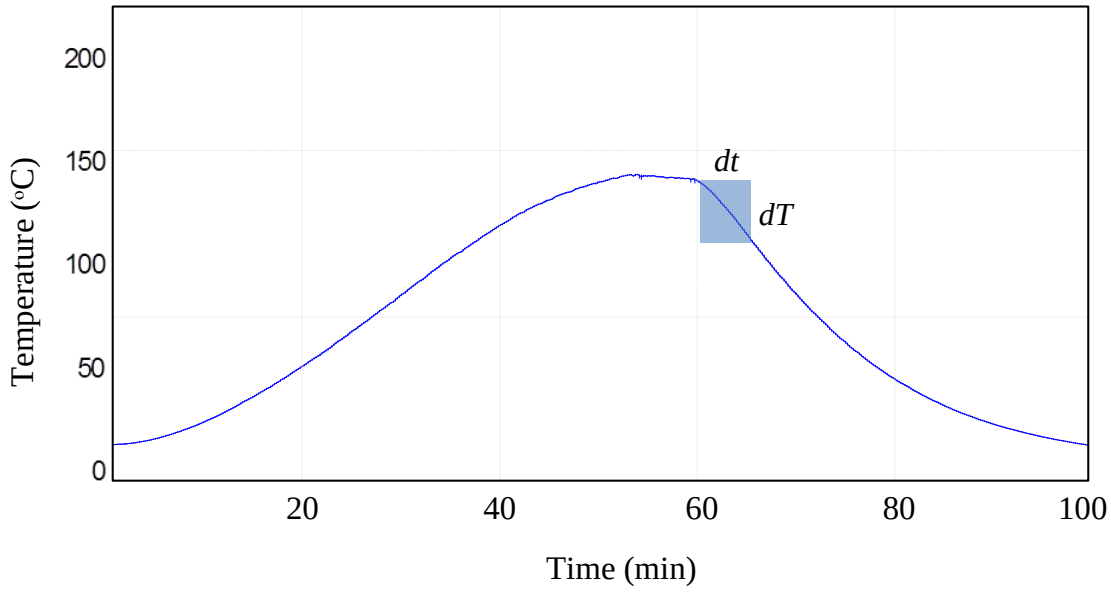

Figure 19 Cooling rate calculation methodology

Table 12 shows the values of the cooling rates obtained for the slow, medium, and fast cooling methods by calculating the slope of the plot part after the temperature starts to drop.

Table 12 Calculated values of cooling rates

Cooling condition	Average Cooling rate (˚C/min)
Slow	0.6
Medium	1.92
Fast	7.5

3.2.4. Specimens' preparation. After processing was done, all specimens were tagged with the orientation angles and the cooling rates to keep track and to eliminate errors in test results (Figure 20).

Figure 20 Cured specimen samples

In order to obtain specimens with the standard dimensions for the tensile test, the processed glassfiber polypropylene plates were cut using a diamond tip blade to ensure very fine cuts. The blade was cooled by water during the cutting process to make sure the temperature of the composites will not rise to a point that will cause the polypropylene to melt. Figures 21 and 22 show the cutting procedure. Figure 23 shows a sample of the final shape of the tensile specimens.

To insure reliability of the research outcomes, two sets of specimens were prepared for every processing condition. All specimens were tagged and prepared for the tensile test as listed in Table 13.

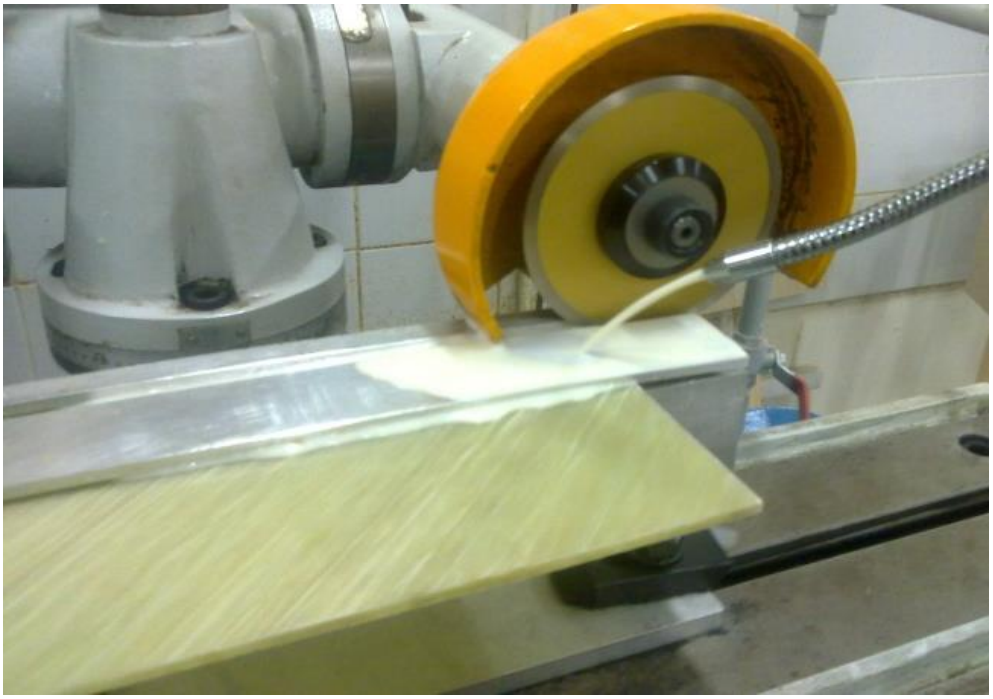

Figure 21 Preliminary specimen cutting

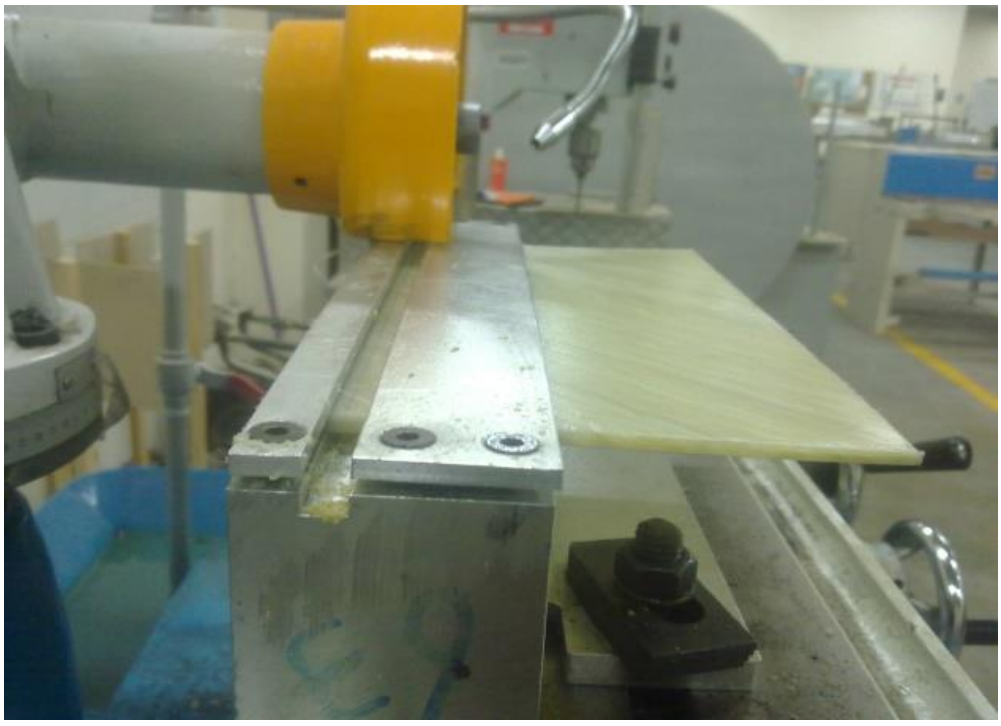

Figure 22 Final specimen cutting

Figure 23 Sample of final shape specimen

Table 13 Tagged specimens list

Condition No.	Tag ID	Orientation angle	Cooling rate (˚C /min)
1	0-S-01	0	Slow (0.6)
	0-S-02	0	Slow (0.6)
2	0-M-01	0	Medium (1.92)
	0-M-02	0	Medium (1.92)
3	0-F-01	0	Fast (7.5)
	0-F-02	0	Fast (7.5)
4	30-S-01	30	Slow (0.6)
	30-S-02	30	Slow (0.6)
5	30-M-01	30	Medium (1.92)
	30-M-02	30	Medium (1.92)
6	30-F-01	30	Fast (7.5)
	30-F-02	30	Fast (7.5)
7	45-S-01	45	Slow (0.6)
	45-S-02	45	Slow (0.6)
8	45-M-01	45	Medium (1.92)
	45-M-02	45	Medium (1.92)
9	45-F-01	45	Fast (7.5)
	45-F-02	45	Fast (7.5)
10	60-S-01	60	Slow (0.6)
	60-S-02	60	Slow (0.6)
11	60-M-01	60	Medium (1.92)
	60-M-02	60	Medium (1.92)
12	60-F-01	60	Fast (7.5)
	60-F-02	60	Fast (7.5)
13	90-S-01	90	Slow (0.6)
	90-S-02	90	Slow (0.6)
14	90-M-01	90	Medium (1.92)
	90-M-02	90	Medium (1.92)
15	90-F-01	90	Fast (7.5)
	90-F-02	90	Fast (7.5)

3.3. Testing Method

In order in get the desired static mechanical properties of the processed specimens (ultimate stress, ultimate strain and modulus of elasticity) tensile tests were performed using an electromechanical Instron testing machine [39].

The applied load was measured by the software from the load cell in the tensile machine and the extension of the specimen while testing was measured using an extensometer placed on the specimen before performing the test as shown in Figure

24. Each specimen's dimension was inserted in the computer to enable the software to calculate the stress applied to the specimen. The cross sectional area of the specimen was calculated from the width and thickness of the specimen, and the gage length was limited to 50 mm which represents distance between the two extensometer blades.

Figure 24 Specimen with extensometer

The test mode was configured using the tensile machine software to be based on the strain rate set to 0.5 mm/min. Figure 25 shows an example of a specimen under the tension test.

3.4. Experimental Results

The tensile machine was programmed to stop the test automatically once it detects a sudden drop of the load applied (signifying specimen failure). The software will then generate the test results in a tabular form that contains the time, load, stress and extension. The output was recorded by the software on time bases (1 record per 0.5 sec); on average rate 2000 records were captured for each test. Figure 26 shows and example of a 45^{o} specimen after failure.

Figure 25 Specimen during tensile stress testing

Figure 26 Example of a 45° specimen after failure

Stress values extracted from the test output were calculated by the tensile machine software. The strain values were calculated based on the extracted extension values from the extensometer and the gage length of the specimen.

Once all stress and strain values were calculated and tabulated, stress vs. strain curves were plotted for each condition separately using Microsoft Excel software. Each graph includes three stress-strain curves: one curve for the first attempt, second curve for the second attempt, and the third curve for the average between the two tests. The desired mechanical properties were extracted from the plotted curves for further analysis. Figure 27 shows an example of the stress vs. strain chart for fiber orientation angle 0^o and cooling rate of 0.6 ^oC/min, all charts for the remaining conditions can be found in the Appendix.

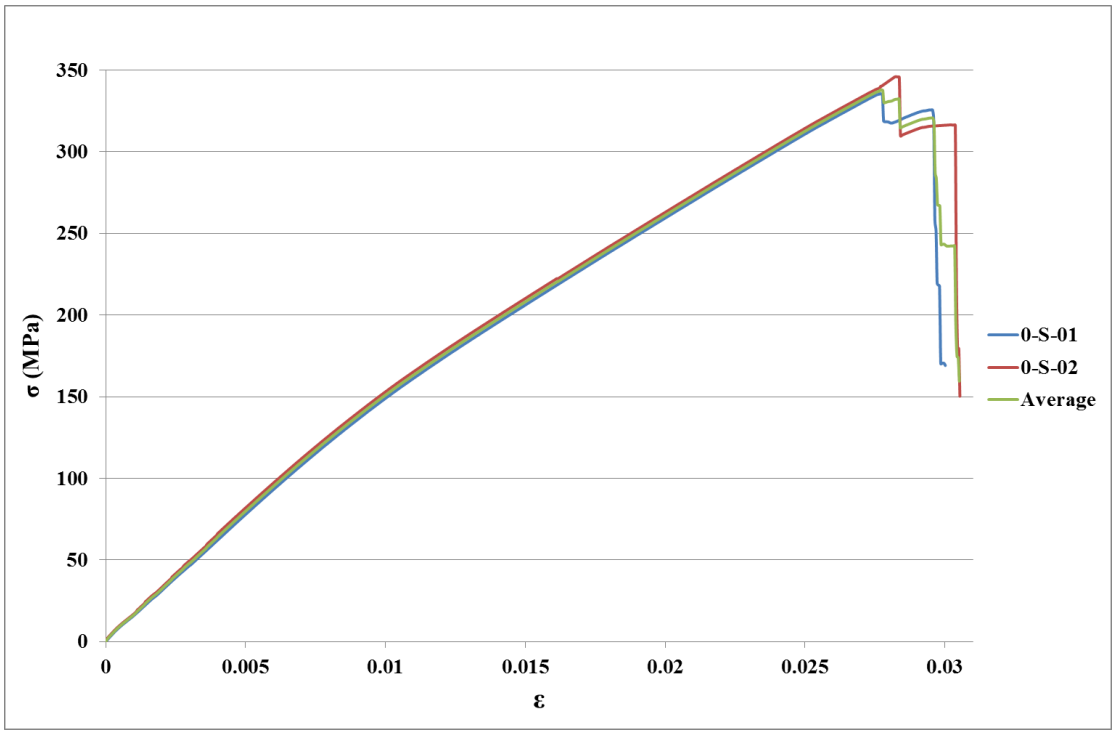

Figure 27 Stress vs. strain curves for 0̊ degrees fiber orientation angle and 0.6 ˚C/min cooling rate

To consider the effect of cooling rate on the mechanical properties of unidirectional laminas, Figures 28 to 32 show the stress-strain curves of different cooling rate values combined in each chart for the same fiber orientation angle.

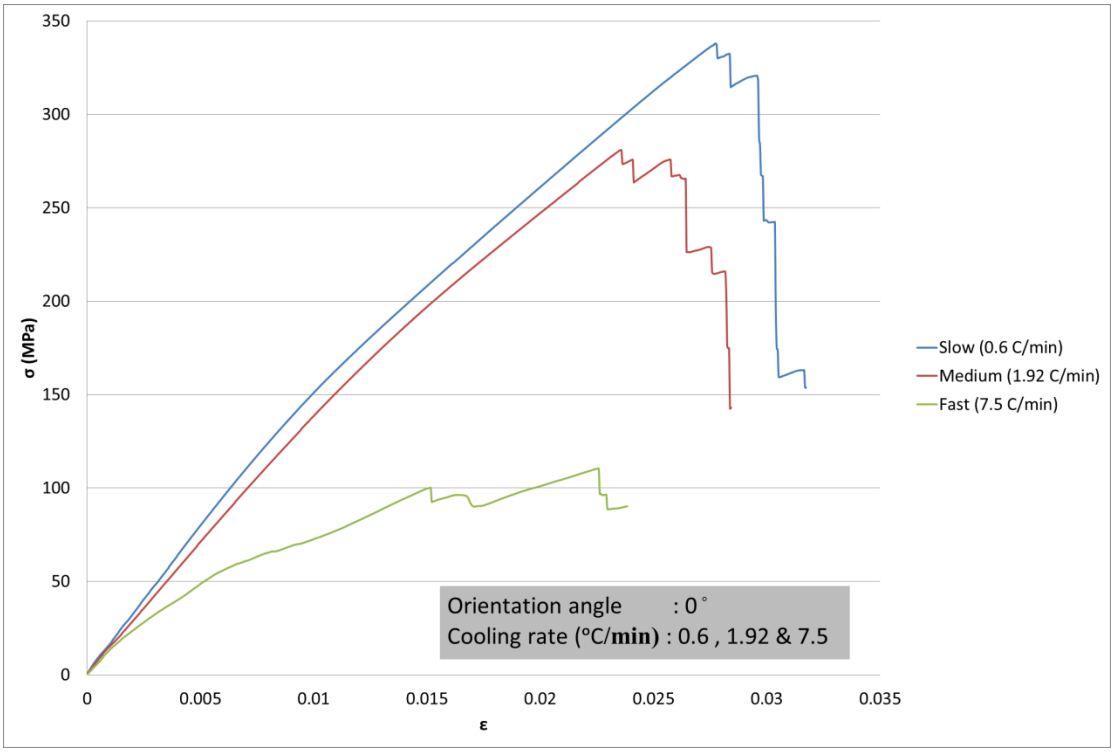

Figure 28 Stress vs. strain curve for three cooling rates and 0 - degrees orientation

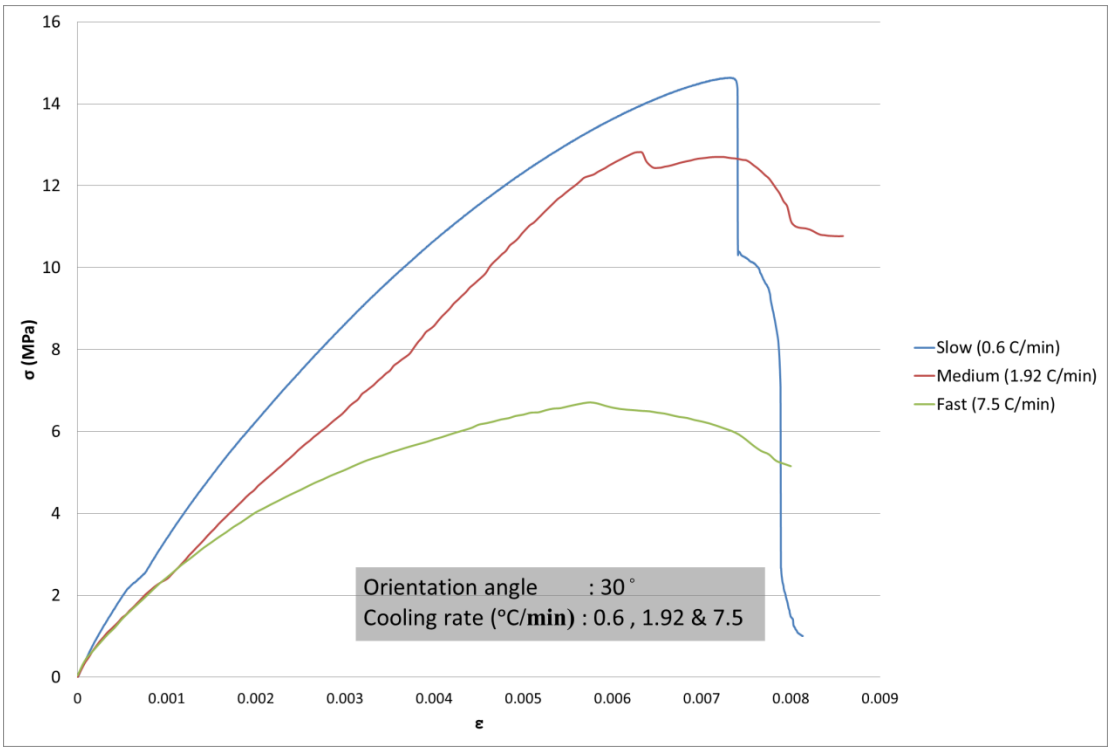

Figure 29 Stress vs. strain curve for three cooling rates and 30 – degrees orientation

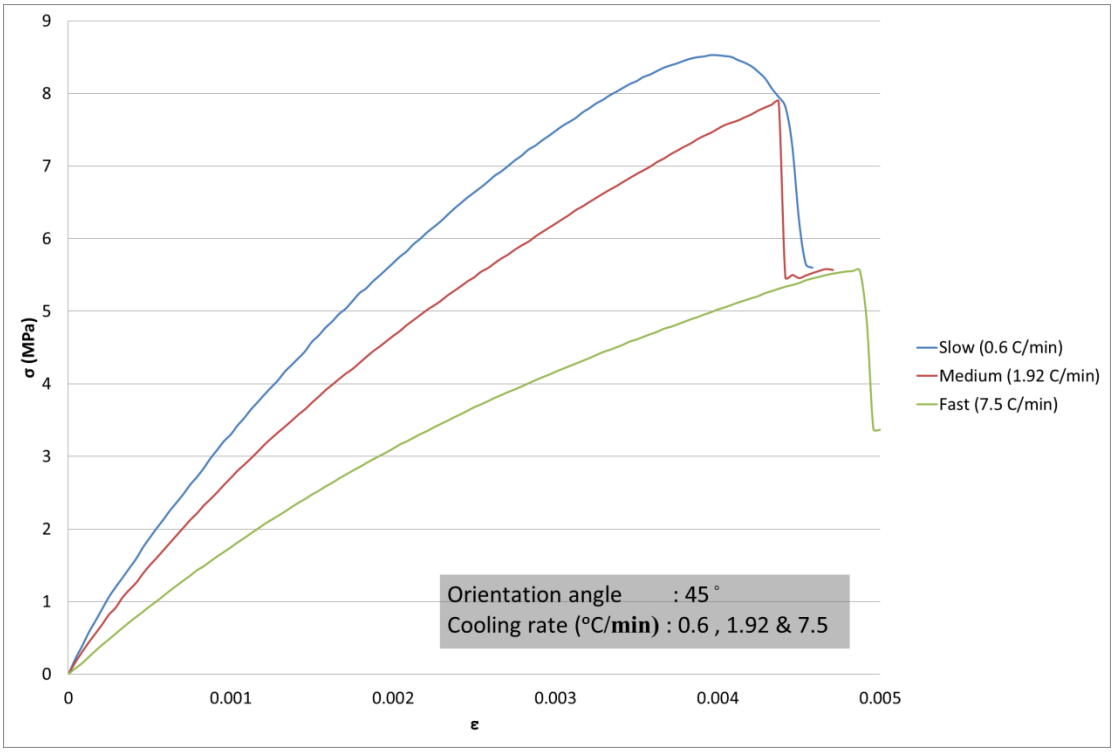

Figure 30 Stress vs. strain curve for three cooling rates and 45 – degrees orientation

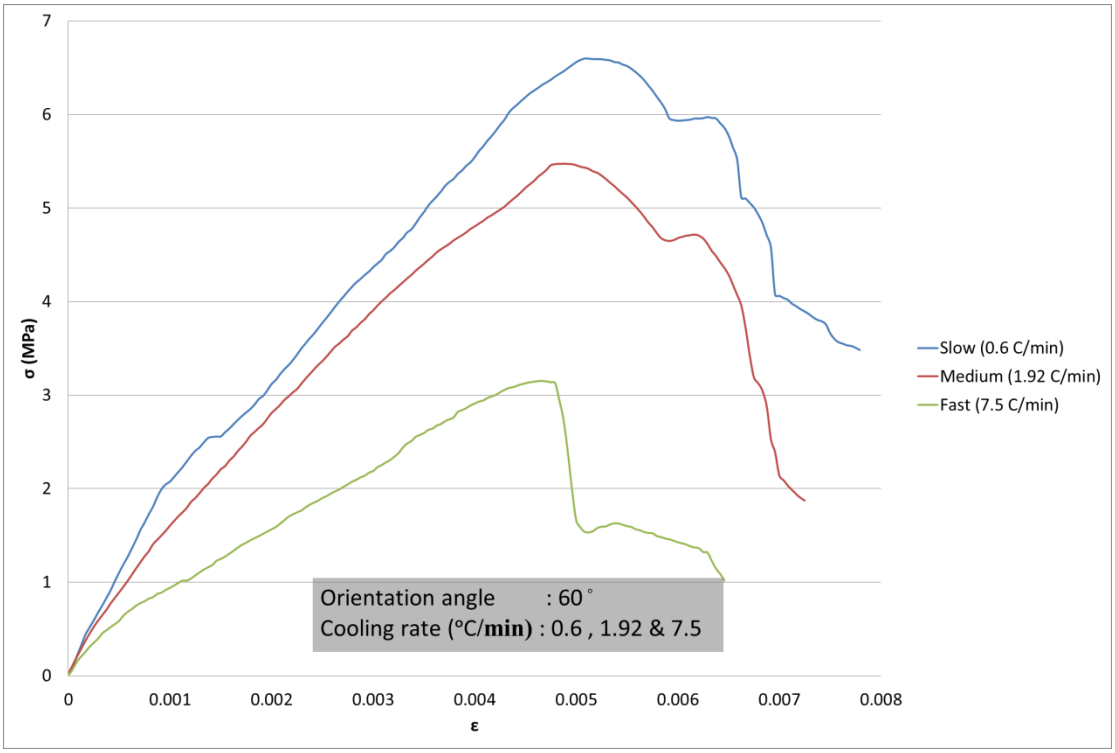

Figure 31 Stress vs. strain curve for three cooling rates and 60 – degrees orientation

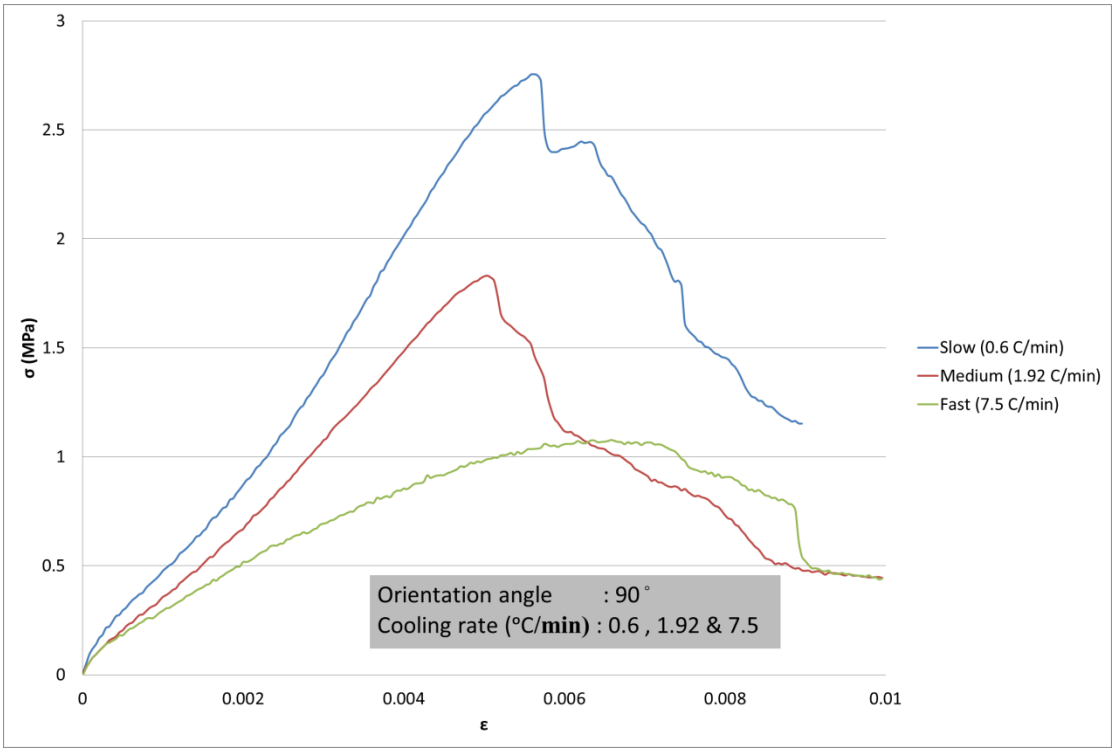

Figure 32 Stress vs. strain curve for three cooling rates and 90 – degrees orientation

The stress-strain curves plotted based on the experimental results have been used to extract some of the mechanical properties to gauge the effect of cooling rate on the properties. Ultimate stress, ultimate strain and modulus of elasticity are the mechanical properties extracted using the following approaches:

- Ultimate stress (σ_u): The maximum stress value in the stress-strain curve
- Ultimate strain (εu): The strain value at ultimate stress
- Modulus of elasticity (*E*): The stress-strain curve slope in the elastic region.

Because all the obtained stress-strain curves were found to have non-linear elastic behaviour, the chord modulus of elasticity, defined based on the ASTM D3039/D3039M standard, was used. The chord modulus of elasticity can be simply defined as the slop of the chord drawn between any two specified points on the stress-strain curve [40] as illustrated in Figure 33. To obtain consistent and comparable results, the chord modulus of elasticity was calculated based on fixed strain range as recommended in the ASTM standard. The recommended strain range is between strain value 0.001 and 0.003 and should has a value of 0.002 (±0.0002). Equation 3.1 was used to calculate the chord modulus of elasticity in this study.

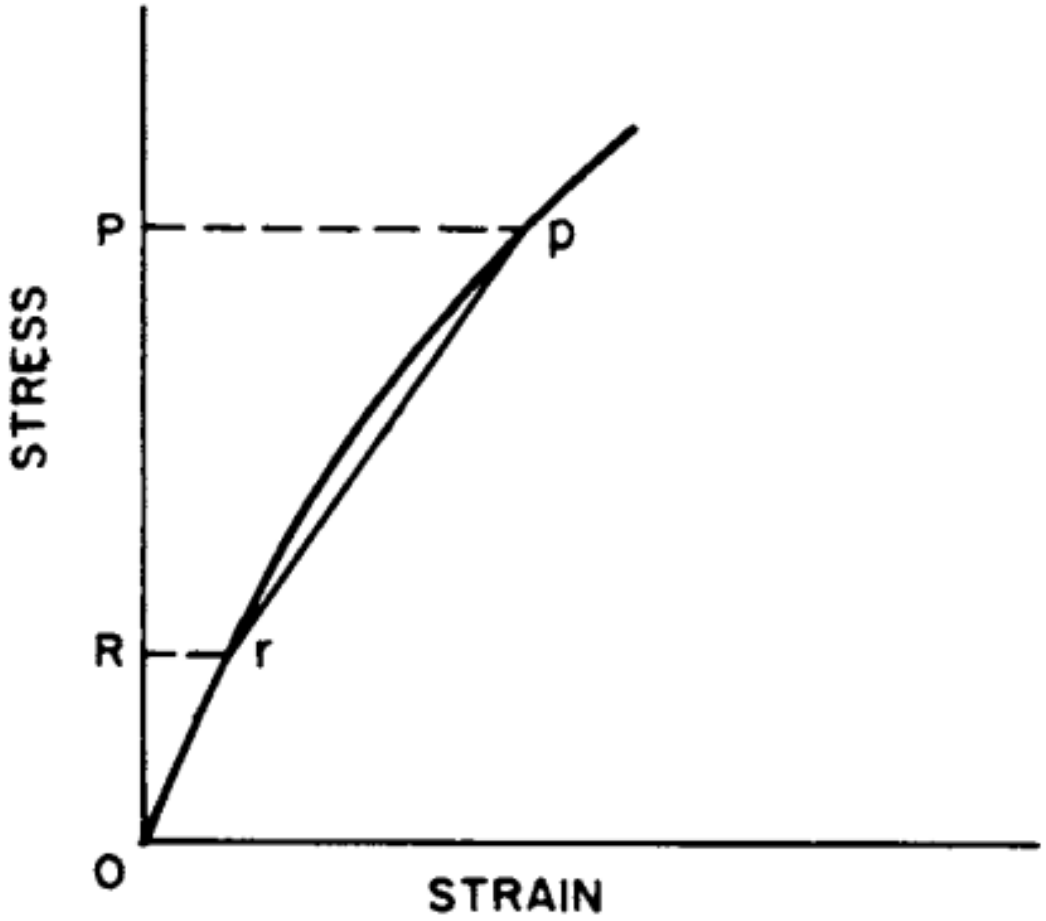

Figure 33 Graphical example of the chord modulus [40]

$$E^{chord} = \frac{\Delta\sigma}{\Delta\varepsilon} \quad (3.1)$$

Where:

E^{chord} = tensile chord modulus of elasticity, GPa

$\Delta\sigma$ = difference in tensile stress between the two strain points, MPa

$\Delta\varepsilon$ = difference between the two strain points, 0.002 (±0.0002).

Figure 34 shows an example of how the ultimate stress, the ultimate strain and the elastic modulus were extracted from the stress-strain charts.

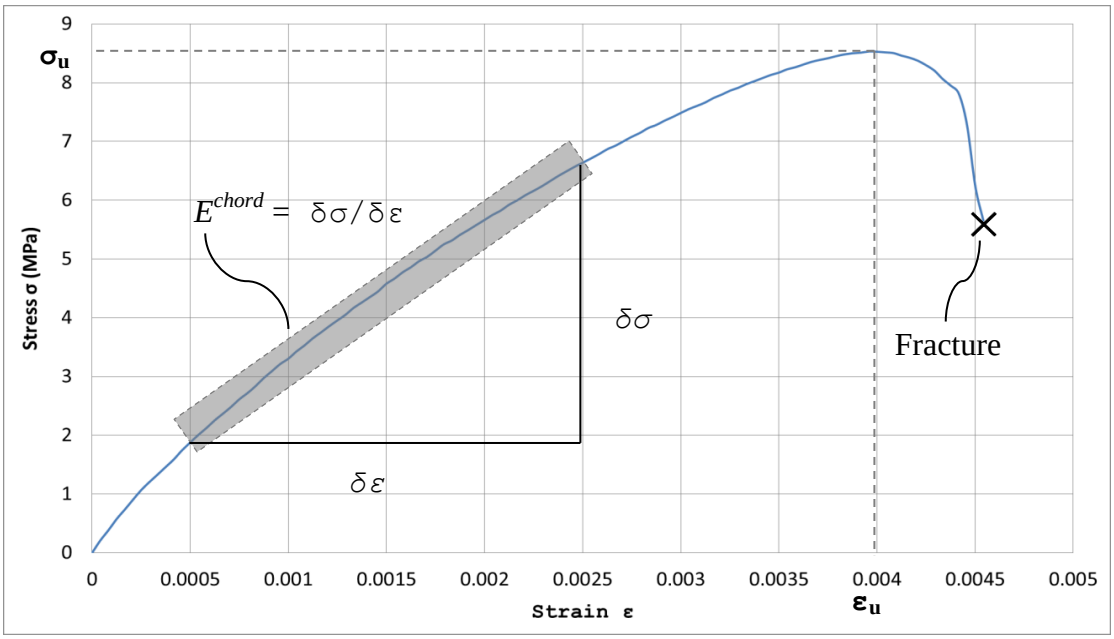

Figure 34 Mechanical properties extraction methodology

Table 14 lists the mechanical properties for all the tested specimens which were extracted from stress-strain curves. As shown, the calculated mechanical properties values variation based on the fiber orientation angles and the cooling rate support the earlier analysis of the stress-strain charts. From the results it can be concluded that the cooling rate mainly affects the modulus of elasticity and the ultimate stress and has minor effect on the ultimate strain.

Figures 35 and 36 show the effect of cooling rates on the ultimate strength and modulus of elasticity separately. The left y-axis in both graphs is used to measure the ultimate stress and modulus of elasticity respectively of the zero degree fiber orientation angle while the right y-axis is used for the ultimate stress and modulus of elasticity of the remaining fiber orientation axes. The results were plotted using two axes due to the big difference in the values of ultimate stress and modulus of elasticity between the zero degree angle and the other angles. The values of the ultimate stress and modulus of elasticity for all conditions represented in Figures 35 and 36 are the average values of the two experimental tests, were the actual experimental values are represented as error bars in the graphs. The resulting trends obtained for the current material were found to be similar to those published in [18] for Ryton and XLC40-66 composites (Table 2 and 3).

Table 14 Mechanical properties extracted from the results of the tested specimens

Cooling Rate (°C/min)	Orientation Angle (Degrees)	Test No.	σ_u (MPa)	ε_u	E (GPa)
0.6	0	1	345.6	0.02837	14.4
		2	335.5	0.02769	14.4
1.92	0	1	285.3	0.02404	11.3
		2	278.8	0.02571	11.2
7.5	0	1	113.3	0.02250	8.91
		2	113.2	0.02467	8.84
0.6	30	1	15.13	0.00721	2.41
		2	14.25	0.00767	2.24
1.92	30	1	13.16	0.00700	1.97
		2	12.99	0.00662	1.75
7.5	30	1	6.400	0.00572	1.49
		2	7.020	0.00575	1.36
0.6	45	1	8.793	0.00400	1.58
		2	8.270	0.00396	1.49
1.92	45	1	7.792	0.00467	1.17
		2	8.229	0.00438	1.32
7.5	45	1	6.154	0.00492	1.01
		2	5.226	0.00475	0.878
0.6	60	1	7.862	0.00521	1.41
		2	7.003	0.00508	1.31
1.92	60	1	5.619	0.00488	1.20
		2	5.292	0.00538	1.09
7.5	60	1	2.737	0.00438	0.764
		2	3.415	0.00504	0.758
0.6	90	1	3.108	0.00546	0.554
		2	2.801	0.00659	0.573
1.92	90	1	2.007	0.00488	0.456
		2	1.764	0.00544	0.409
7.5	90	1	1.026	0.00579	0.169
		2	1.152	0.00721	0.141

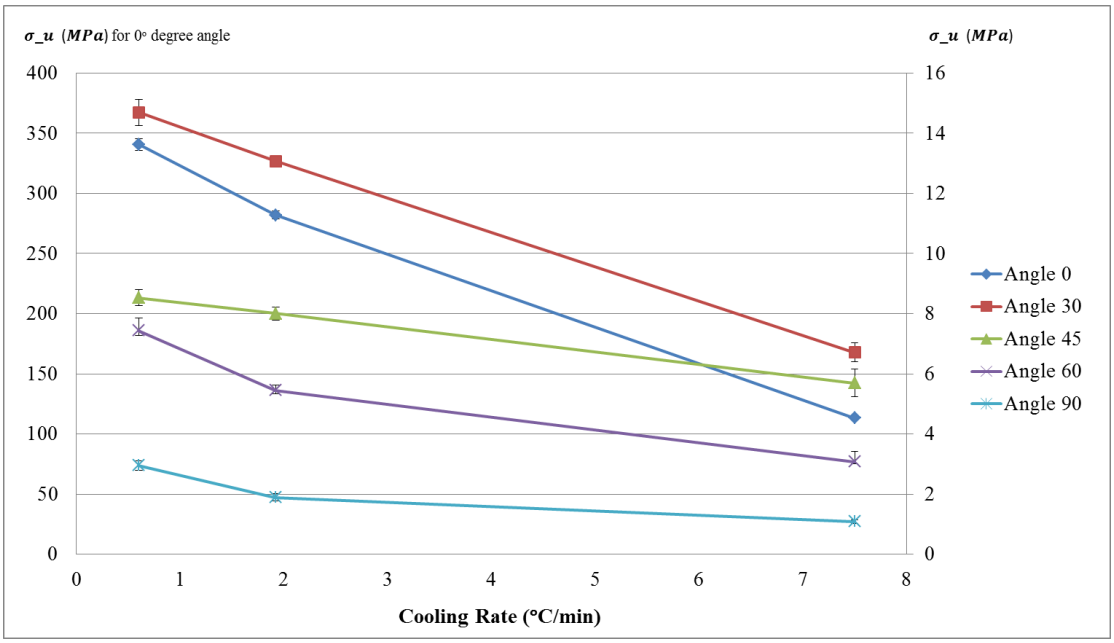

Figure 35 Effect of cooling rate on ultimate strength

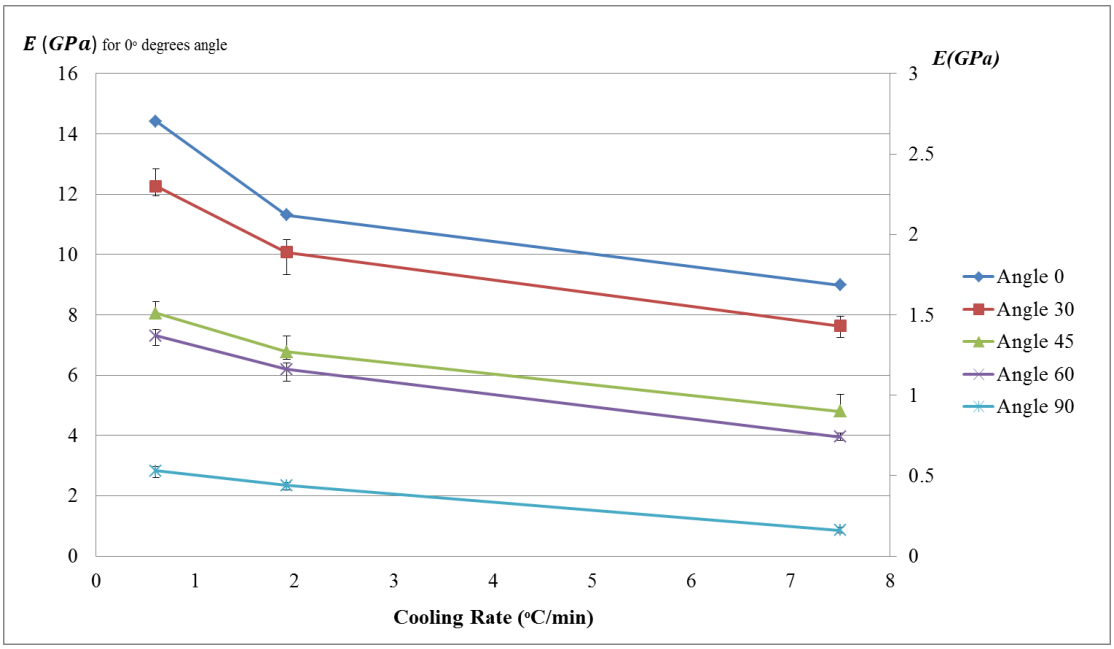

Figure 36 Effect of cooling rate on modulus of elasticity

Chapter 4: Predicting the Mechanical Behavior using ANN

In this chapter, ANN will be used to predict the mechanical properties of unidirectional glassfiber polypropylene as a function of the cooling rate. Neuro Solution software [41] will be used for this purpose. There are three basic phases in neural network analysis, starting with building the neural network, then training the network on existing data, and last testing the network for accuracy and making predictions. The input layer of the ANN will contain three inputs; the cooling rate, the fiber orientation angle, and the experimental stress value, while the output layer contains single output which is the strain value.

4.1. Network Build-up

To build up a Neural Network several parameters should be set such as neural model, number of hidden layers, number of neurons in each layer, etc.; every type of dataset needs a different combination of these parameters to build up the network. To reach the best possible and accurate results for a specific data set, building the network should be carried out varying all the network parameters. To achieve the best network model that can predict this study conditions accurately, the effect of a number of network parameters (number of hidden layers, number of neurons, and number of epochs) on the network performance was investigated. The effect of each of these parameters was investigated individually by developing number network models with the same parameters but differs in the parameter that needs to be investigated. Tables 15, 16 and 17 summarise the outcomes of each parameter been investigated on three different conditions. Table 15 shows the effect of varying the number of hidden layers on the mean square error between predictions and experiments, Table 16 shows the effect of varying the number of neurons on the mean square error, and Table 17 shows the effect of using a different number of epochs on the mean square error.

In Table 15, predictions obtained from ANN with one and two hidden layers are compared. For all these cases, the number of neurons in each hidden layer was kept at 50 neurons and the ANN was trained for 1000 Epochs. The most accurate prediction was obtained using 2 hidden layers for all three conditions.

Table 15 Effect of varying the number of hidden layers on the mean square error between experiments and the ANN predictions

Condition		No. of hidden layers	Mean square error
Fiber orientation angle (degree)	Cooling rate (^{o}C/min)		
0	1.92	1	0.003925
		2	0.0003755
30	7.5	1	0.004230
		2	0.0003357
90	0.6	1	0.005126
		2	0.0004780

In Table 16, predictions obtained from networks containing 2 hidden layers are compared. For all these cases, the ANN was trained for 1000 Epochs. The most accurate prediction was obtained using 50 neurons.

Table 16 Effect of varying the number of neurons on the mean square error between the experiments and the ANN predictions

Condition		No. of neurons	Mean square error
Fiber orientation angle (degree)	Cooling rate (^{o}C/min)		
0	1.92	10	0.0009863
		25	0.0005256
		50	0.0003755
		75	0.0004023
30	7.5	10	0.0008925
		25	0.0005628
		50	0.0003357
		75	0.0003964
90	0.6	10	0.001739
		25	0.0008362
		50	0.0004780
		75	0.0006027

Table 17, predictions obtained from networks containing 2 hidden layers with 50 neurons in each hidden layer are compared. It was observed that when the neural network been trained for more than 1000 iteration the mean square error increased. The most accurate prediction was obtained by training the network for 1000 epochs.

Table 17 Effect of varying the number of training epochs on the mean square error between experiments and ANN predictions

Condition		No. of epochs	Mean square error
Fiber orientation angle (degree)	Cooling rate (^{o}C/min)		
0	1.92	200	0.0053821
		500	0.0003925
		1000	0.0003755
		2000	0.0128342
30	7.5	200	0.0053429
		500	0.0003826
		1000	0.0003357
		2000	0.0136482
90	0.6	200	0.0076352
		500	0.0005182
		1000	0.0004780
		2000	0.0100263

Table 18 shows all the network parameters combinations that have been attempted to build the neural networks, where the combination highlighted in green is the one gave the most accurate testing results as will be shown in section 4.3.

The selected neural model selected is the Multilayer perceptrons (MLPs), consists of layered feedforward networks typically trained with static backpropagation. These networks have found their way into countless applications requiring static pattern classification. Their main advantage is that they are easy to use, and that they can approximate any input/output map. The key disadvantages are that they train slowly, and require lots of training data (typically three times more training samples than network weights) [41].

Regarding the No. of hidden layers, 2 hidden layers showed more accurate results than single hidden layer during training. Three hidden layers were classified as unpractical as it can take very long time to train. Fifty neurons in each hidden layer were found to give the best outcome.

Learning from the data is the essence of neuro computing. Backpropagation is by far the most common form of learning. Here it is sufficient to say that the weights are changed based on their previous value and a correction term. The learning rule is the means by which the correction term is specified [41]. Using the RProp Algorithm for both hidden layers resulted with the most accurate results among the other learning rules.

Table 18 network parameters combinations tested

Neural Model	No. of hidden layers	No. of Neurons		Learning Rule in		No. of Epochs
		Layer 1	Layer 2	Layer 1	Layer 2	
Multilayer Perceptron (MLPs)	1	20	20	Step	Step	200
Generalized Feed Forward		30	30	Momentum	Momentum	
Modular Neural Network		40	40			
Jordan/Elman Network		50	50	Conjugate-Gradient	Conjugate-Gradient	500
Principal Component Analysis (PCA)		60	60			
RBF/GRNN/PNN Network	2	70	70	Levenberg-Marquardt	Levenberg-Marquardt	1000
Self-Organizing Feature Map Network		80	80	RProp	RProp	
Time-Lag Recurrent Network		90	90	Quickprop	Quickprop	
Recurrent Network		100	100			
CANFIS Network (Fuzzy Logic)		200	200	DeltaBarDelta	DeltaBarDelta	1100
Support Vector Machine		500	500			

4.2. Network Training

Training the network should be done on the data set collected from the tensile tests results for all different conditions (cooling rates and fiber orientation angles) except the condition that the network will be tested for. In another words both the input data including cooling rate, fiber orientation angle, and stress and the output data (strain) of a single condition will be excluded from the training dataset. The excluded data then used to check the accuracy of the predicted data after testing the network. This will help to obtain a good prediction model that can be used for future application of fiber glass polypropylene processing, it has been decided to train the network to predict the stress-strain curves for all experimented conditions, and that will allow extracting the mechanical properties from the stress strain curves. Figure 37 shows a sample of the data set used for training.

After gathering all data and placing them in single data set, training data and testing data should be defined to enable the network to use the training data as base to apply the learning algorithm to predict the testing data and compare it with the actual data and measure the error.

4.3. Network Testing

Testing the Network is the second phase of neural network analysis process, in this phase the network will predict the data that has been defined as testing data during the network build up phase (same data excluded during the training phase). In order to generalize this prediction on all conditions included in this study and to insure applicability of the neural network among wide range of cooling rates and orientation angle, the testing process has been carried out using the same network parameters on all experimental conditions, in other words all possible combinations of cooling rates and orientation angles have been tested one at a time. As a result the predicted data used to plot stress strain curves for all conditions that has been compared with the experimental stress train curve to enable accuracy calculations. Table 19 shows all the tests that have been carried out for all conditions with the predicted stress strain curves.

Figures (38 to 52) show experimental vs. predicted stress strain curves for all processing conditions where the mechanical properties have been extracted from.

	A	B	C	D
1	Cooling rate	orientation	Stress	Strain
2	0.6	0	0	***0***
3	0.6	0	0.77908	***0.00004185***
4	0.6	0	1.59012	***0.0000825***
5	0.6	0	2.41931	***0.00012465***
6	0.6	0	3.21945	***0.0001659***
7	0.6	0	4.00914	***0.00020925***
8		0	4.76238	
4187	1.92			***0.0104125***
4188	1.92	30	2.71031	***0.0010825***
4189	1.92	30	2.81361	***0.00112555***
4190	1.92	30	2.91335	***0.0011674***
4191	1.92	30	3.01432	***0.00120805***
4192	1.92	30	3.10981	***0.0012496***
4193	1.92	30	3.20499	***0.00129115***
4194	1.92	30	3.29998	***0.0013342***
4195	1.92	30	3.38613	***0.00137575***
6395	1.92			***0.0028653***
6396	1.92	90	1.17948	***0.0028747***
6397	1.92	90	1.20585	***0.00291715***
6398	1.92	90	1.21775	***0.0029596***
6399	1.92	90	1.24106	***0.00299995***
6400	1.92	90	1.25292	***0.0030409***
6401	1.92	90	1.28538	***0.00308305***
6402	1.92	90	1.30416	***0.0031258***
6403	1.92	90	1.32526	***0.00316735***
6404	1.92	90	1.34258	***0.0032083***
6405	1.92	90	1.35523	***0.00324955***
6406	1.92	90	1.37397	***0.0032908***
6407	1.92	90	1.39528	***0.00333415***
6408	1.92	90	1.41769	***0.0033751***
6409	1.92	90	1.43259	***0.00341665***

Figure 37 Dataset used to train the ANN

Table 19 Stress-strain curves predicted using ANN for all considered conditions

Test Code	Cooling rate (˚C/min)	Orientation angle	Stress vs. Strain
ANN_0_S	0.6	0	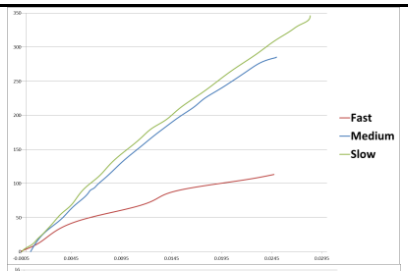
ANN_0_M	1.92	0	
ANN_0_F	7.5	0	
ANN_30_S	0.6	30	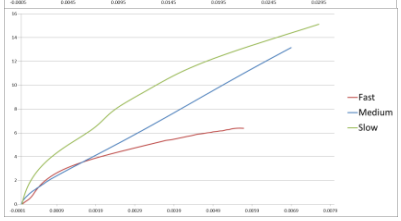
ANN_30_M	1.92	30	
ANN_30_F	7.5	30	
ANN_45_S	0.6	45	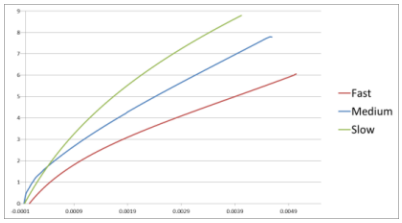
ANN_45_M	1.92	45	
ANN_45_F	7.5	45	
ANN_60_S	0.6	60	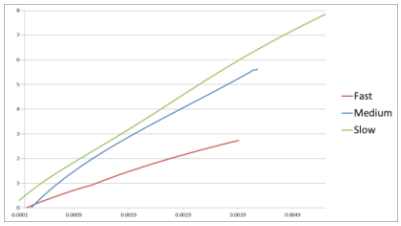
ANN_60_M	1.92	60	
ANN_60_F	7.5	60	
ANN_90_S	0.6	90	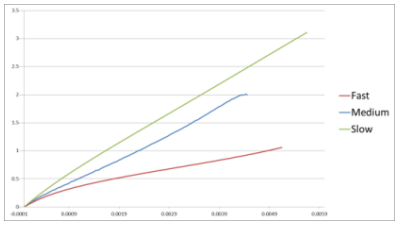
ANN_90_M	1.92	90	
ANN_90_F	7.5	90	

For fiber orientation angle 0̊ and slow cooling rate (Figure 38), the predicted and the experimental stress-strain curves are almost matching, however the predicted curve starts at a negative strain value which could be due to training the network model on huge number of various conditions dataset.

For the condition showed in Figure 39, the predicted and the experimental stress-strain curves match and show similar behavior as the slow cooling rate of the

same fiber orientation angle. Once again an initial value of strain was observed in the predicted stress-strain curve.

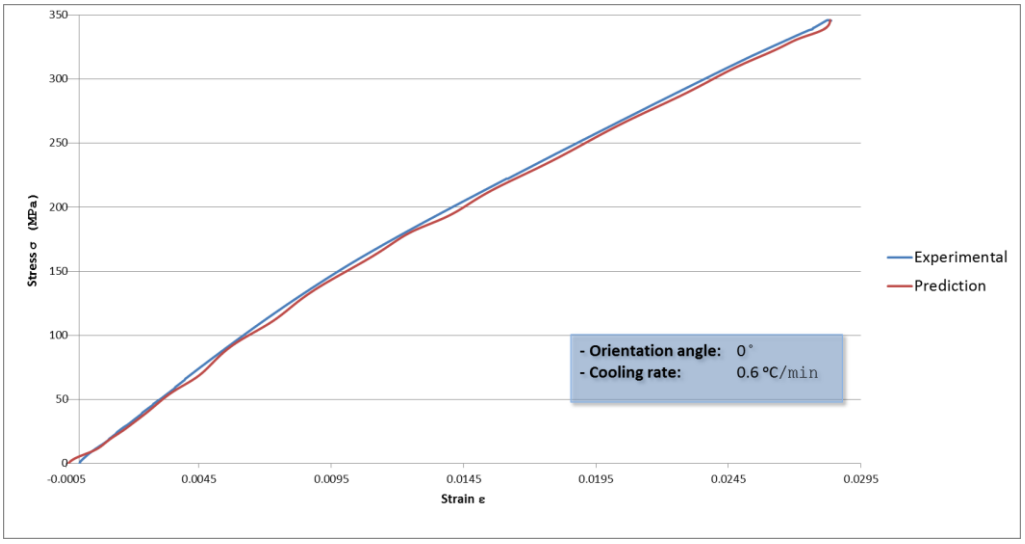

Figure 38 Experimental vs. predicted stress strain curve for 0 degrees orientation angle and slow cooling rate

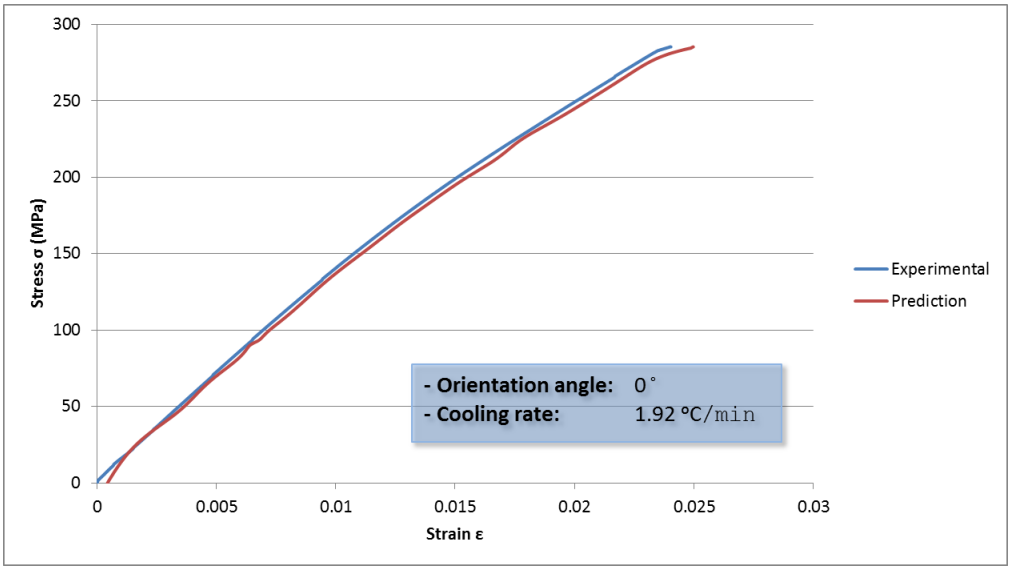

Figure 39 Experimental vs. predicted stress strain curve for 0 degrees orientation angle and medium cooling rate

For the fast cooling rate condition of the 0° degrees fiber orientation angle specimens (Figure 40), the predicted stress-strain curve follows the experimental stress-strain curve pattern with an almost constant shift. In this case, the prediction obtained follows the variations in curvature obtained in the experimental curve. Those variations could be the result of inaccuracies in the tensile test. Once again a slight strain value is predicted at zero tensile stress.

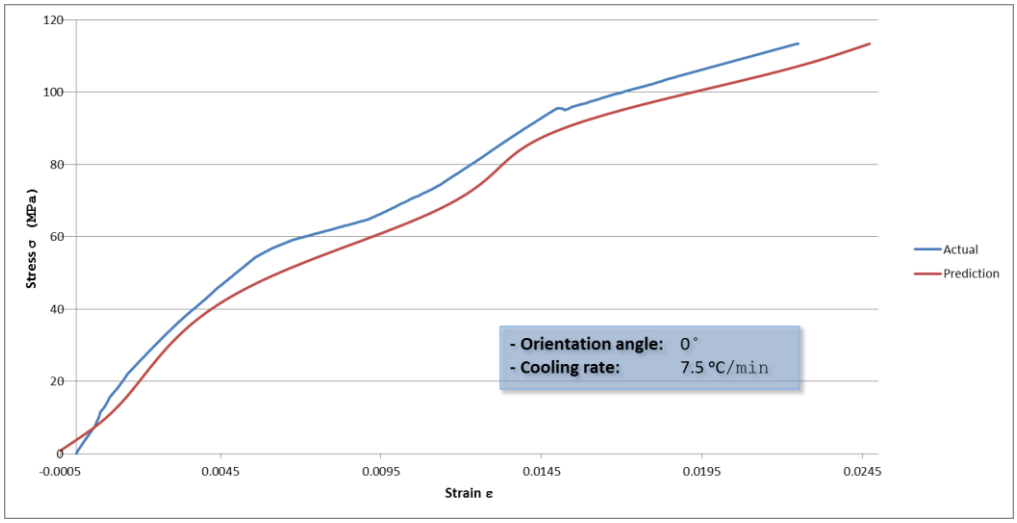

Figure 40 Experimental vs. predicted stress strain curve for 0 degrees orientation angle and fast cooling rate

For 30̊ degrees fiber orientation angle and slow cooling rate condition (Figure 41), the predicted and the experimental stress-strain curves were found to deviate from one another early in the test then, once again, just before failure.

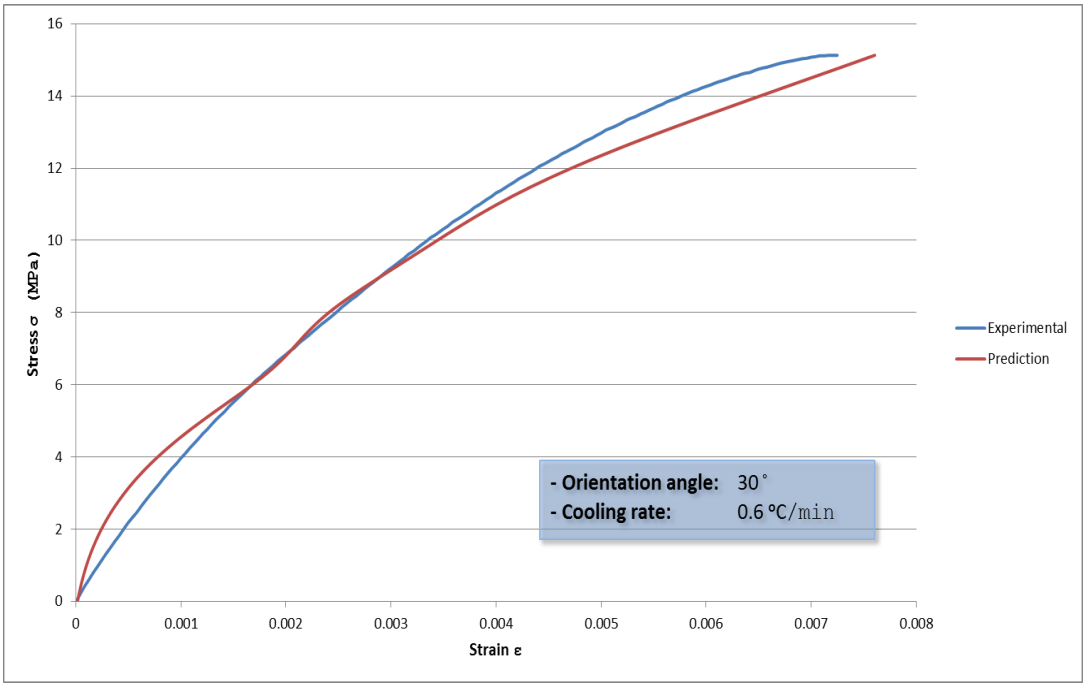

Figure 41 Experimental vs. predicted stress strain curve for 30 degrees orientation angle and slow cooling rate

Once again, for the 30o specimens manufactured using the medium cooling rate (Figure 42), the predicted stress-strain curve shows a variation compared to the experimental midway through the stress/strain range.

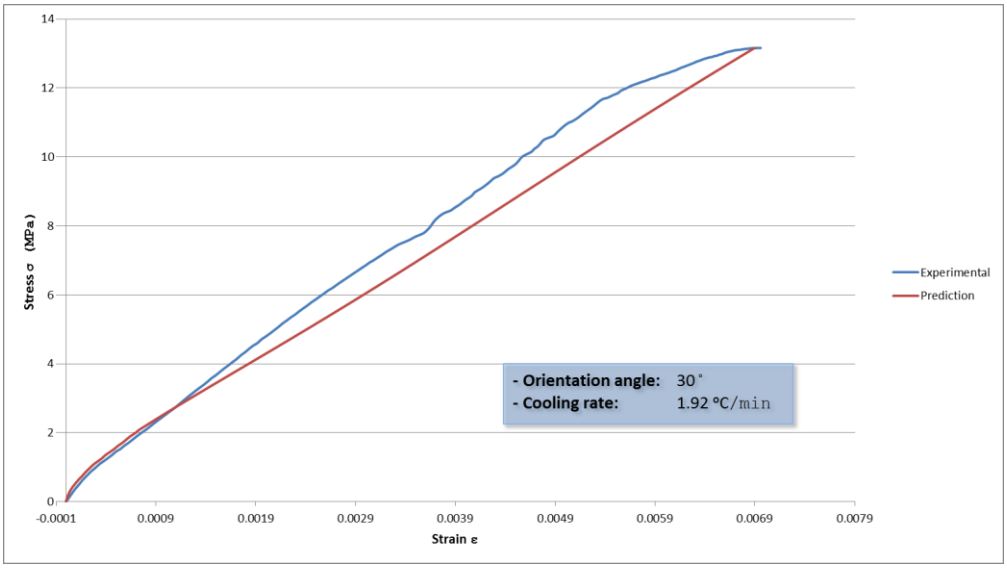

Figure 42 Experimental vs. predicted stress strain curve for 30 degrees orientation angle and medium cooling rate

The condition shown in Figure 43 follows a slightly different pattern than the medium and slow cooling rate of the same fiber orientation angle. In this case, the predicted stress-strain curve matches the experimental stress-strain curve at the first third and last third of the curve, and deviates at the middle third.

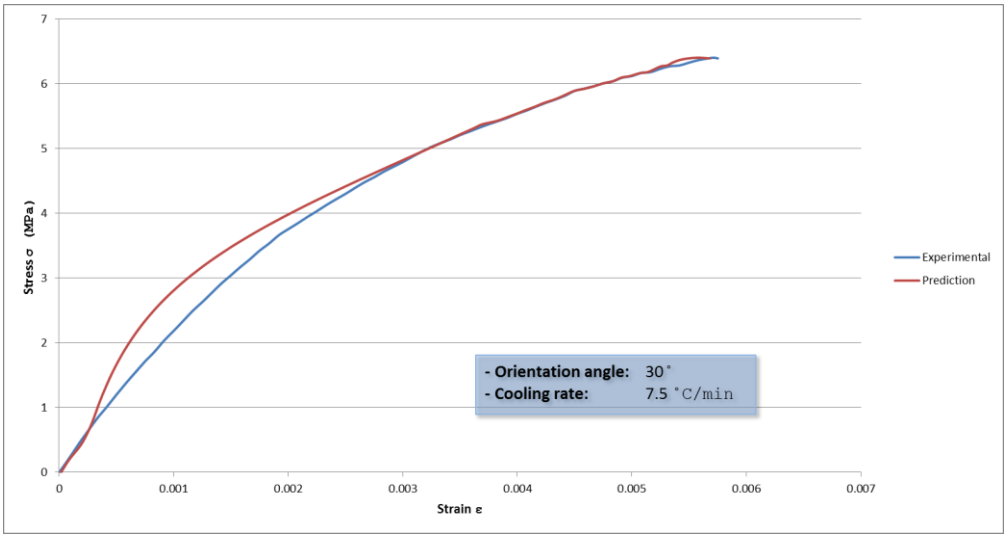

Figure 43 Experimental vs. predicted stress strain curve for 30 degrees orientation angle and fast cooling rate

Specimens with 45° degrees orientation angle show better predicted stress-strain curves visually that the 30° degrees orientation angle conditions. For the slow cooling rate condition (Figure 44), the predicted curve matches the experimental behavior early in the test, a deviation is then observed between predictions and experiments, to match again at failure.

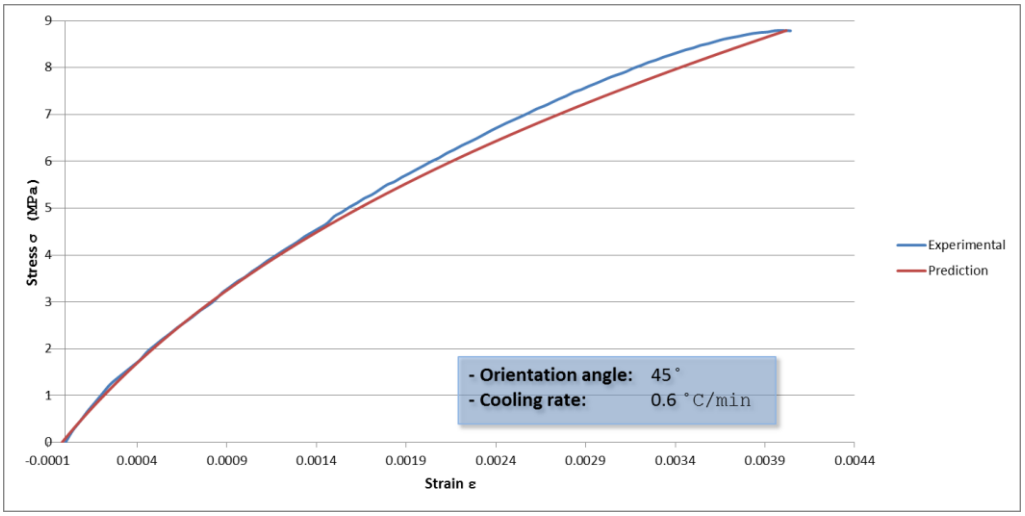

Figure 44 Experimental vs. predicted stress strain curve for 45 degrees orientation angle and slow cooling rate

The predicted and experimental stress-strain curves illustrated in Figure 45 show a gap between the curves for the low stress and strain ranges to almost match for the rest of test. It is worth mentioning that a small negative strain value was predicted at the start of the test which could be attributed to the same reason mentioned for the 0o specimens.

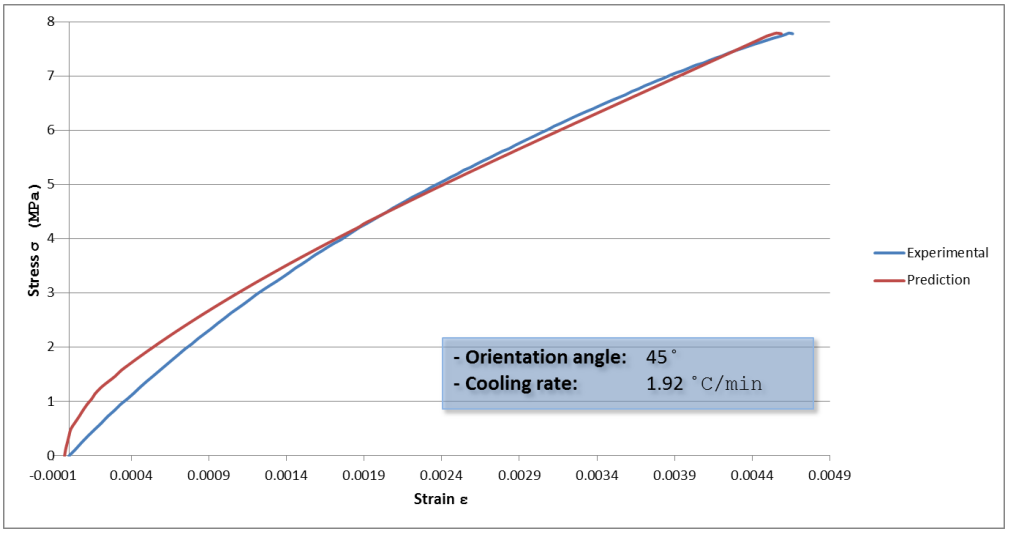

Figure 45 Experimental vs. predicted stress strain curve for 45 degrees orientation angle and medium cooling rate

The fast cooling rate condition of 45° degrees fiber orientation angle specimens (Figure 46) showed a similar behavior of the slow cooling rate of the same angle with respect the observed gap between the predicted and experimental stress-strain curves.

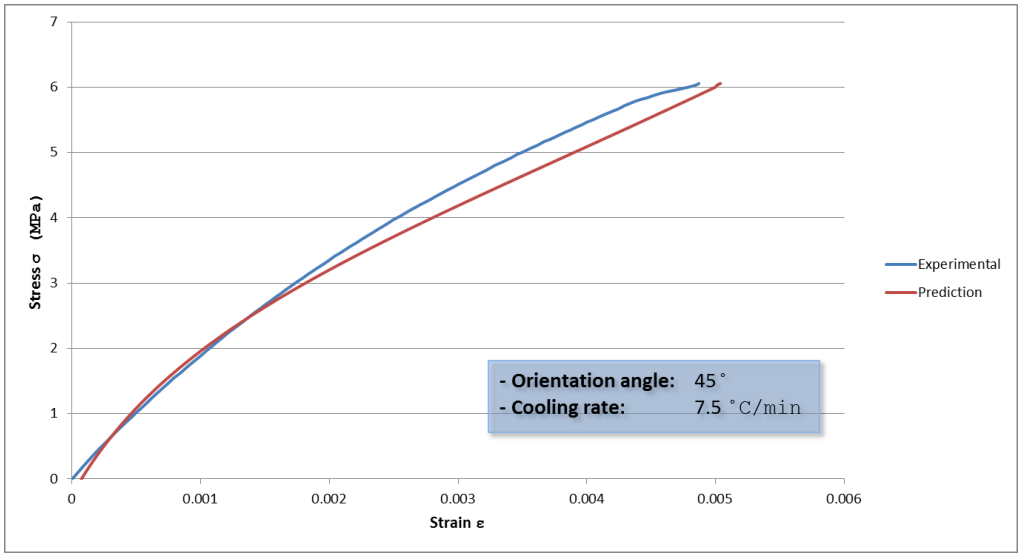

Figure 46 Experimental vs. predicted stress strain curve for 45 degrees orientation angle and fast cooling rate

For experiments conducted on specimens with fiber orientation angles above 45°, the curves became rougher unlike the predicted curves. This could be due to the fact that the majority of the network training dataset was provided from 0°, 30°, and 45° degrees orientation angles including the three cooling rates of each angle. For 60o specimens with slow cooling rate (Figure 47), the predicted curve did not follow the slight curvature observed in the experimental data. Once again, a negative strain was predicted at the zero stress level.

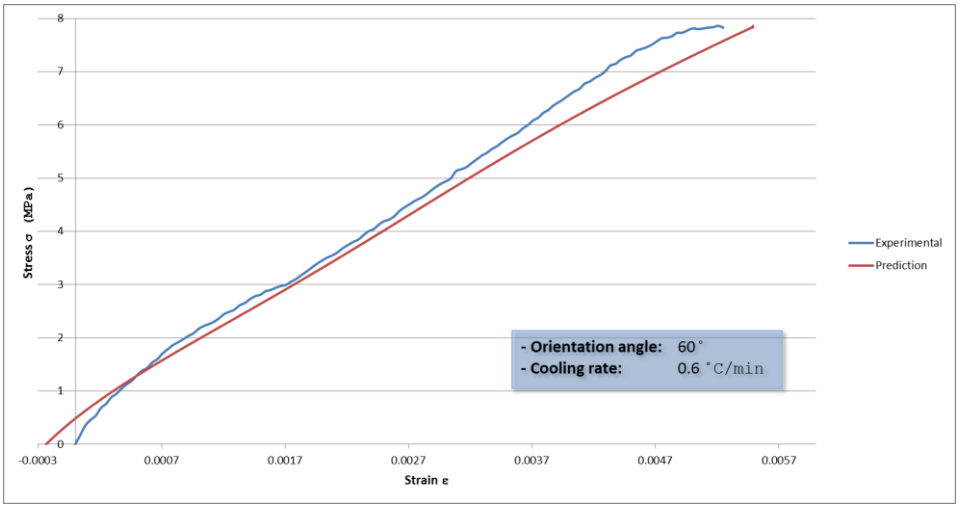

Figure 47 Experimental vs. predicted stress strain curve for 60 degrees orientation angle and slow cooling rate

Although the predicted stress-strain curve looks smoother than the experimental curve for the 60̊ degrees fiber orientation angle and medium cooling rate (Figure 48); experimental and predicted behavior match during the central part of the curve but a slight variation is observed at the start and the end of the experiment. A positive strain value was observed at the start of the experiment.

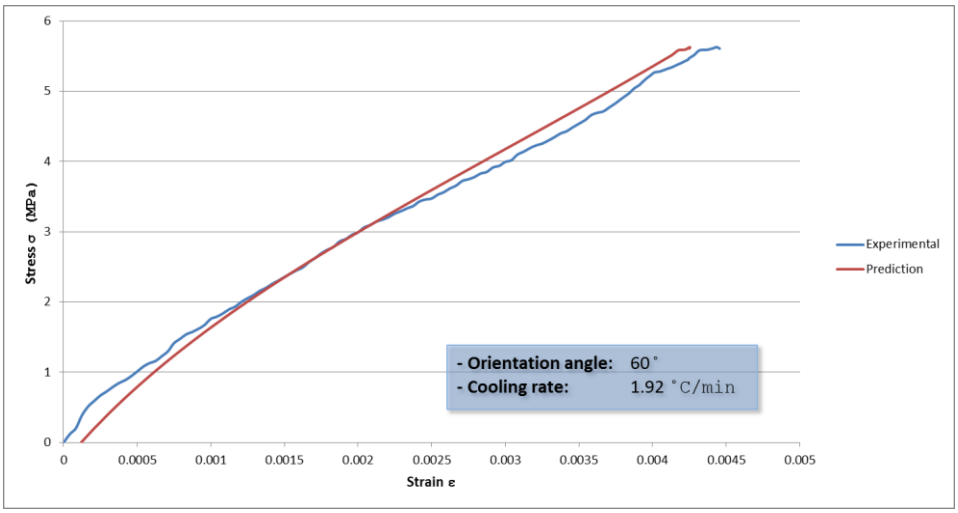

Figure 48 Experimental vs. predicted stress strain curve for 60 degrees orientation angle and medium cooling rate

The fast cooling rate condition of 60̊ fiber orientation angle specimen (Figure 49) predicted stress-strain curve found to be close to the experimental curve for most of the curve but a little gap started to occur at the end of the curve.

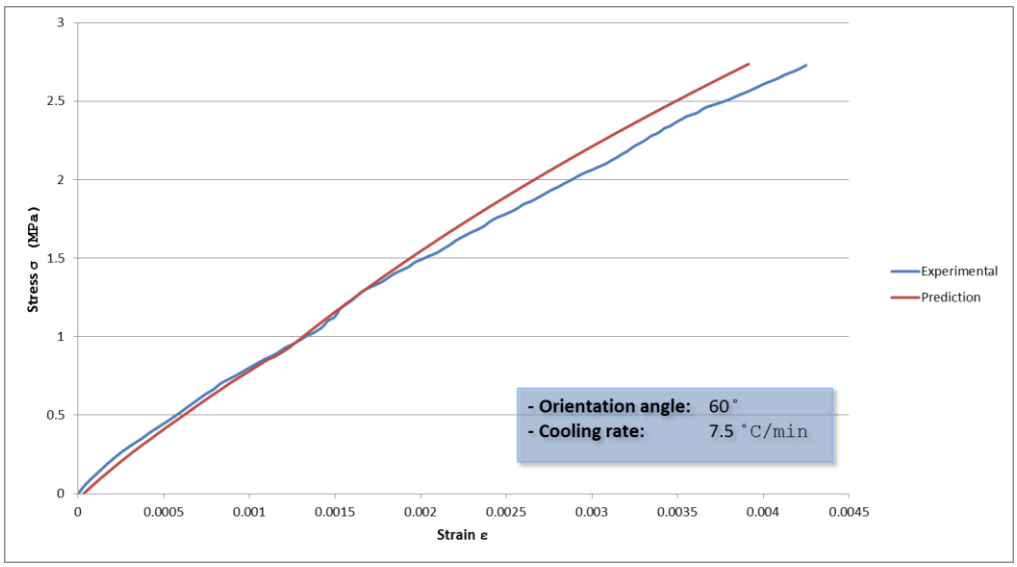

Figure 49 Experimental vs. predicted stress strain curve for 60 degrees orientation angle and fast cooling rate

The 90̊ degrees fiber orientation angle prediction behavior found to be similar to the 60̊ degrees orientation angle for all cooling rates conditions, where the predicted stress-strain curves are smoother than the experimental curves. For the slow cooling rate condition (Figure 50), the ANN over-predicted the experimental behavior early in the text and under-predicted the behavior later on.

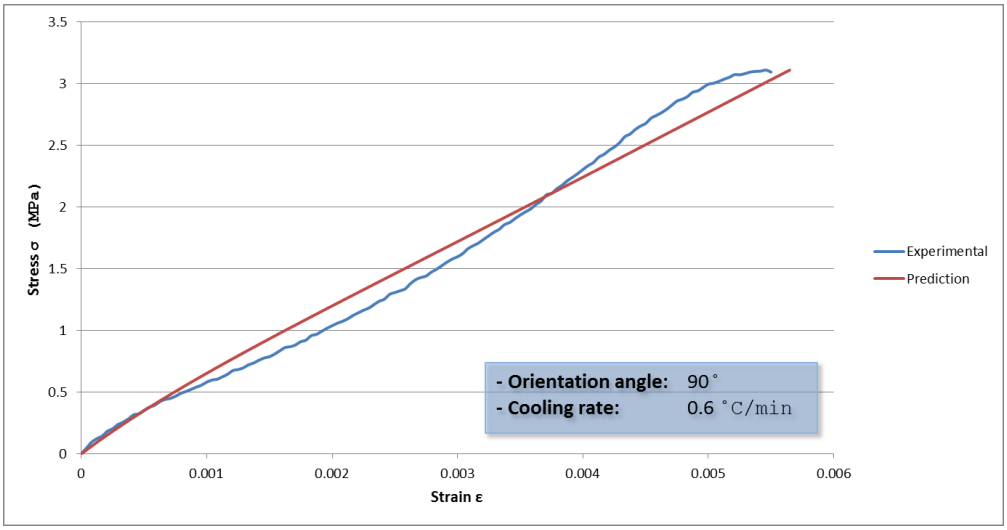

Figure 50 Experimental vs. predicted stress strain curve for 90 degrees orientation angle and slow cooling rate

The predicted stress-strain curve of the condition illustrated in Figure 51 follows the same pattern of the experimental stress-strain curve. It is noticed also that the gap between both curves increases as the strain value increases.

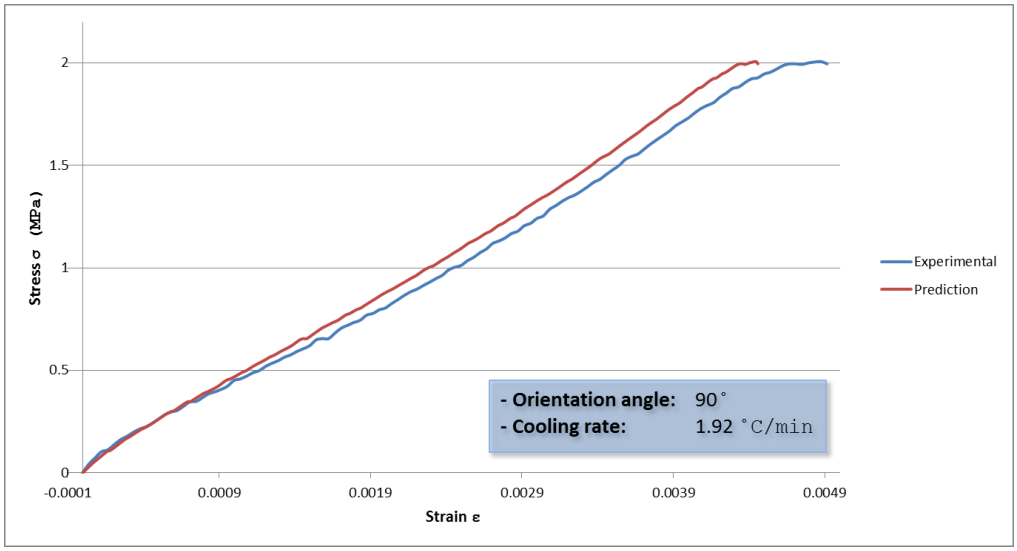

Figure 51 Experimental vs. predicted stress strain curve for 90 degrees orientation angle and medium cooling rate

In the condition shown in Figure 52, it is shown that the predicted stress-strain curve overlaps with the experimental stress-strain curve at multiple locations; a gap is however observed between the two curves midway through the test and close to failure.

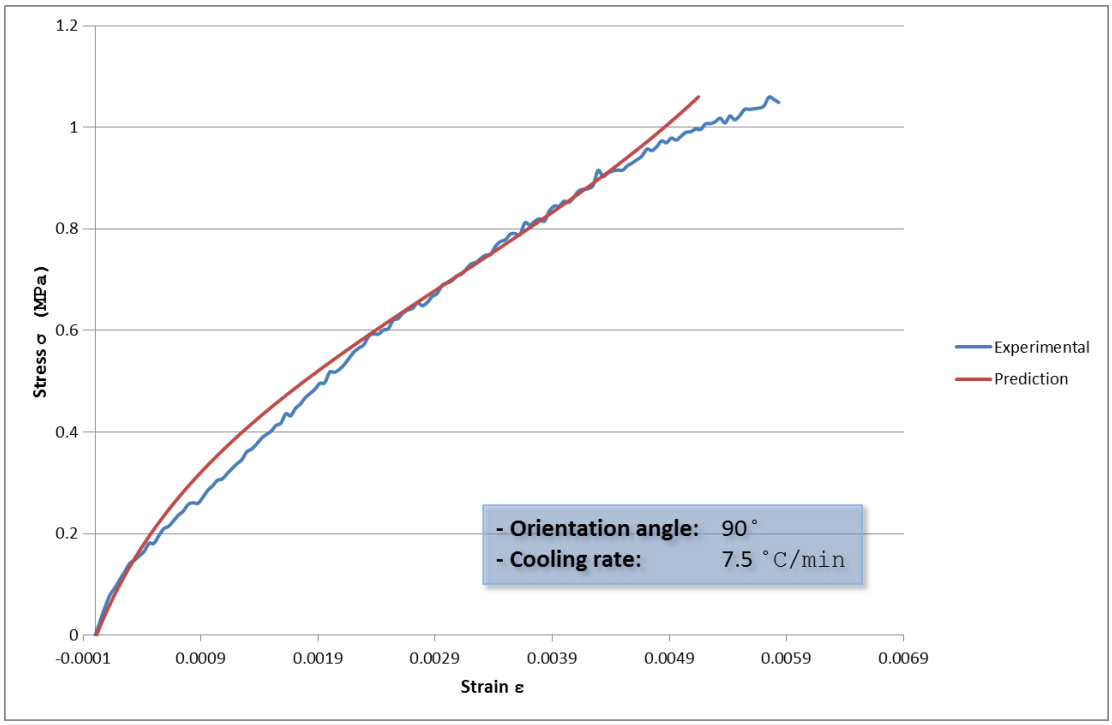

Figure 52 Experimental vs. predicted stress strain curve for 90 degrees orientation angle and fast cooling rate

4.4. ANN Accuracy

The neural network accuracy can be calculated in different ways, but it has been decided for this study to calculate the accuracy by comparing the experimental mechanical properties with the predicted ones, this will help studying the ability of the built neural network to predict the mechanical properties of the glass-fiber polypropylene composites for various cooling rates.

Table 20 summarizes the experimental and the predicted mechanical properties as a function of processing conditions and shows the % accuracy of the results obtained in each case.

Table 20 Mechanical properties values for experimental vs. predicted results

Inputs			Outputs					
Cooling Rate	Orientation Angle	Ultimate Strength	Ultimate Strain			Modulus of Elasticity (GPa)		
(˚C/ min)	(Degrees)	(MPa)	Experimental	Prediction	Accuracy	Experimental	Prediction	Accuracy
0.6	0	345.6	0.02837	0.02834	99.87%	14.4	14.3	99.13%
1.92	0	285.3	0.02404	0.02498	96.09%	11.3	11.1	98.08%
7.5	0	113.3	0.02250	0.02470	90.18%	8.99	8.87	98.71%
0.6	30	15.13	0.00721	0.00761	94.48%	2.30	2.29	99.24%
1.92	30	13.16	0.00691	0.00690	99.77%	1.89	1.85	97.92%
7.5	30	6.40	0.00572	0.00558	97.70%	1.43	1.42	99.34%
0.6	45	8.79	0.00400	0.00402	99.52%	1.51	1.52	99.34%
1.92	45	7.78	0.00466	0.00459	98.43%	1.27	1.28	99.44%
7.5	45	6.06	0.00487	0.00504	96.53%	0.899	0.908	98.96%
0.6	60	7.86	0.00521	0.00549	94.58%	1.37	1.35	98.64%
1.92	60	5.63	0.00444	0.00425	95.93%	1.16	1.18	98.11%
7.5	60	2.74	0.00425	0.00361	85.05%	0.738	0.749	98.67%
0.6	90	3.11	0.00546	0.00565	96.51%	0.531	0.534	99.46%
1.92	90	2.01	0.00488	0.00445	91.22%	0.441	0.455	98.95%
7.5	90	1.08	0.00658	0.00523	79.43%	0.155	0.155	99.64%

Chapter 5: Conclusion and Future Work

Static behavior of unidirectional polypropylene glassfiber composite material manufactured under various cooling rates was investigated.

- As expected, cooling rate significantly affects the mechanical properties of thermoplastic composites. It was found that as cooling rate increased, the ultimate stress, ultimate strain and the modulus of elasticity decreased; this behavior was observed for the various fiber orientation angles. This behavior also matches results published in the literature for various thermoplastic-based composites.
- Artificial Neural Networks (ANN) were used to predict the mechanical properties of the material under a variety of cooling rate conditions. To our knowledge, this is the first time that ANN have been used for such purpose.
- It was concluded that developing an ANN model using Multilayer Perceptrons (MLPs) neural model including two hidden layers each contained 50 neurons and using the RProp training algorithm for both hidden layers resulted in the most accurate results among the other network parameters combinations.
- It was also found that using ANN to predict the mechanical properties of polypropylene glassfiber composites could significantly save cost and time for the material designers, as the value of resulting prediction error was relatively small.

Possible extension of this study might include one or more of the following areas:

- Using larger number of cooling conditions.
- Studying the effect of other processing conditions (curing temperature, curing pressure, time at curing temperature).
- Investigating additional ANN parameters to obtain a more accurate prediction.
- Extending the study to multidirectional laminates.
- Include investigating the effect of the cooling conditions on the fatigue properties of the material.

References

[1] A. Brent Strong “History of Composite Materials Opportunities and Necessities,” Brigham Young University, 2006.

[2] David Roylance “Introduction to Composite Materials,” Department of material science and engineering, Massachusetts Institute of Technology, Cambridge, 2000.

[3] M.H.R. Jen and C.H. Lee “Strength and Life in Thermoplastic Composite Laminates under Static and Fatigue Loads. part 1: Experimental,” *Int. J. Fatigue*, vol. 20, pp. 605 - 615, 1998.

[4] N.L. Hancox “High Temperature High Performance Composites,” *Advance Materials and Manufacturing Process*, vol. 3, pp. 359 - 389, 1988.

[5] N. Abilash and M. Sivapragash “Environmental Benefits of Ecofriendly Natural Fiber Reinforced Polymeric Composite Materials,” *International Journal of Application or Innovation in Engineering & Management*, vol. 2, pp. 54 - 56, 2013.

[6] https://www.creativemechanisms.com/blog/all-about-polypropylene-pp-plastic (accessed January 5th, 2017).

[7] C. Hennaf-Gardin and M.C. Lafarie-Frenot “Fatigue Behavior on Thermoset and Thermoplastic Cross-Ply Laminates,” *Composites*, vol. 23, pp. 109 - 116, 1992.

[8] M.C. Lafarie-Frenot and F. Touchard “Comparative in-Plane Shear Behavior of Long-Carbon-Fiber Composites with Thermoset or Thermoplastic Matrix,” *Composite Science and Technology*, vol. 52, pp. 417 - 425, 1994.

[9] H.H. Kausch. *Advanced Thermoplastic Composites: Characterized Processing*, Hanser Gardner, 1993.

[10] J.A.E. Manson, T.L. Schneider, and J.C. Seferis “Press-Forming of Continuous-Fiber-Reinforced Thermoplastic Composites,” *Polymer Composites*, vol. 11, pp. 114 - 120, 1990.

[11] H. David, A.M. James, Q. Lawrence, and L. Robert “High Speed Processing of Thermoplastic Composites for Oilfield Pipe and Tubular Applications,” http://www.automateddynamics.com/technical-paper (accessed January 25th, 2017). PR 15, 2000.

[12] P.Y.B. Jar, and H.H. Kausch "The Influence of Molding conditions on Delamination Behavior of Carbon-Fiber/PEEK Composites," *Composite Science and Technology*, vol. 52, pp. 349 - 359, 1994.

[13] P. Davies, W.J. Cantwell, P.Y. Jar, H. Richard, D.J. Neville and H.H. Kausch "Cooling Rate Effects in Carbon Fiber/PEEK Composites," *Composite Materials: Fatigue and Fracture*, vol. 32, pp. 775 - 785, 2001.

[14] J.A.E. Manson and J.C. Seferis "Process Simulated Laminate (PSL): A Methodology for Internal Stress Characterization in Advanced Composite Materials," *Journal of Composite Materials*, vol. 26, pp. 405 - 431, 1992.

[15] H.Wafai, G. Labineau, A. Yudhanto, M. Mulle, W. Schijve, and N. Verghese "Effects of the cooling rate on the shear behavior of continuous glass fiber/impact polypropylene composites (GF-IPP)," Composites, vol. 91, pp. 41 – 52, 2016.

[16] A. Tregub, H. Harel, G. Marom and C. Migliaresi "The Influence of Thermal History on the Mechanical Properties of PEEK Matrix Composite Materials," *Composites Science and Technology*, vol.48, pp. 185 - 190, 1993.

[17] A. Tregub, H. Harel and G. Marom, "Thermal Treatment Effects on the Crystallinity and the Mechanical Behavior of Carbon Fiber/PEEK Composites," *Journal of Materials Science Letter*, vol. 13, pp. 329 - 331, 1994.

[18] J. Deporter and D.G. Baird "The Effects of Thermal History on the Structure/Property Relationship in Polyphenylenesulfide/Carbon Fiber Composites," Polymer Composites, vol. 14, pp. 201 - 213, 1993.

[19] P. Davies and W.J. Cantwell "Fracture of Glass/PP Laminates: Influence of Cooling Rate after Molding," *Composites*, vol. 25, pp. 869 - 877, 1994.

[20] F. Perrin, M.N. Bureau, J. Denault and J.I. Dickson "Mode I Interlaminar Crack Propagation in Continuous Glassfiber/Polypropylene Composites: Temperature and Molding Condition Dependence," *Composites Science and Technology*, vol. 63, pp. 597 - 607, 2003.

[21] M.N. Bureau, F. Perrin, J. Denault and J.I. Dickson "Interlaminar Fatigue Crack Propagation in Continuous Glass Fiber/Polypropylene Composites," *Internal Journal of Fatigue*, vol. 24, pp. 99 - 108, 2002.

[22] D. Frihi, A. Layachi, S. Gherib, G. Stoclet, K. Masenelli-Varlot, H. Satha, and R. Seguela "Crystallization of Glass-Fiber-Reinforced Polyamide 66 Composites: Influence of Glass-Fiber Content and Cooling Rate," *Composites Science and Technology*, vol. 130, pp. 70 – 77, 2016.

[23] M. Regis, A. Bellare, T. Pascolini, and P. Bracco "Characterization of Thermally Annealed PEEK and CFR-PEEK Composites: Structure-Properties Relationships," *Polymer Degradation and Stability*, vol. 136, pp. 121 – 130, 2017.

[24] H. El Kadi "Modeling the Mechanical Behavior of Fiber-Reinforced Polymeric Composite Materials using Artificial Neural Networks – A Review," *Composite Structures*, vol. 73, pp. 1 - 23, 2006.

[25] M.D. Guyton and C. Arthur. *Human Physiology and Mechanisms of Disease.* Philadelphia: WB Saunders, 1987.

[26] http://slideplayer.com/slide/5127883 (accessed January 5th, 2017).

[27] http://nutritionwonderland.com/2009/06/understanding-bodies-serotonin-connection-between-food-and-mood (accessed January 25th, 2017).

[28] https://www.researchgate.net/figure/259537828_fig4_Figure-2-Schematic-diagram-of-a-three-layer-ANN23 (accessed January 5th, 2017).

[29] R.M.V. Pidaparti and M.J. Palakal "Material Model for Composites using Neural Networks," *AIAA Journal*, vol. 31, pp. 1533 - 1535, 1993.

[30] F. Aymerich and M. Serra "Prediction of the Fatigue Strength of Composite Laminates by Means of Neural Network," *Key Eng Mater*, vol. 144, pp. 231 - 40, 1998.

[31] Y. Al-Assaf and H. El Kadi "Fatigue Life Prediction of Unidirectional Glass Fiber/Epoxy Composite Laminae using Neural Networks," *Composite Structures*, vol. 53. pp. 65 - 71, 2001.

[32] H. El Kadi and Y. Al-Assaf "Prediction of the Fatigue Life of Unidirectional Glass Fiber/Epoxy Composite Laminae using Different Neural Network Paradigms," *Composite Structures*, vol. 55. pp. 239 - 246, 2002.

[33] H. El Kadi and Y. Al-Assaf "Energy-Based Fatigue Life Prediction of Fiberglass/Epoxy Composites using Modular Neural Networks," *Composite Structures*, vol. 57, pp. 85 - 89, 2002.

[34] Z. Zhang and K. Friedrich "Artificial Neural Networks Applied to Polymer Composites: A Review," *Composites Science and Technology*, vol. 63, pp. 2029 - 2044, 2003.

[35] Z. Jiang, Z. Zhang and K. Friedrich "Prediction of Wear Properties of Polymer Composites with Artificial Neural Networks," *Composites Science and Technology*, vol. 67, pp. 168 - 176, 2007.

[36] R. Mishra, J. Malik, I. Singh, and J.P. Davim "Neural Network Approach for Estimating the Residual Tensile Strength after Drilling in Unidirectional Glass Fiber Reinforced Plastic Laminates," *Materials and Design*, vol. 31, pp. 2790 – 2795, 2010.

[37] M.O. Shabani, A. Mazahery, M.R. Rahimipour, and M. Razavi "FEM and ANN Investigation of A356 Composites Reinforced with B_4C Particulates," *Journal of King Saud University – Engineering Sciences*, vol. 24, pp. 107 – 113, 2012.

[38] http://www.imhotepcomposites.co.uk (accessed January 5th, 2017).

[39] http://www.instron.us (accessed January 5th, 2017).

[40] ASTM International Standard, "Standard Test Method for Young's Modulus, Tangent Modulus, and Chord Modulus," Pennsylvania, United State, 2011.

[41] NeuroSolutions software version 7.1.1.1, 2016. Available from: http://www.neurosolutions.com.

Appendix

The appendix includes the stress-strain curves obtained from the tensile tests performed on all glassfiber polypropylene specimens manufactured with different fiber orientation angles manufactured under different cooling rates.

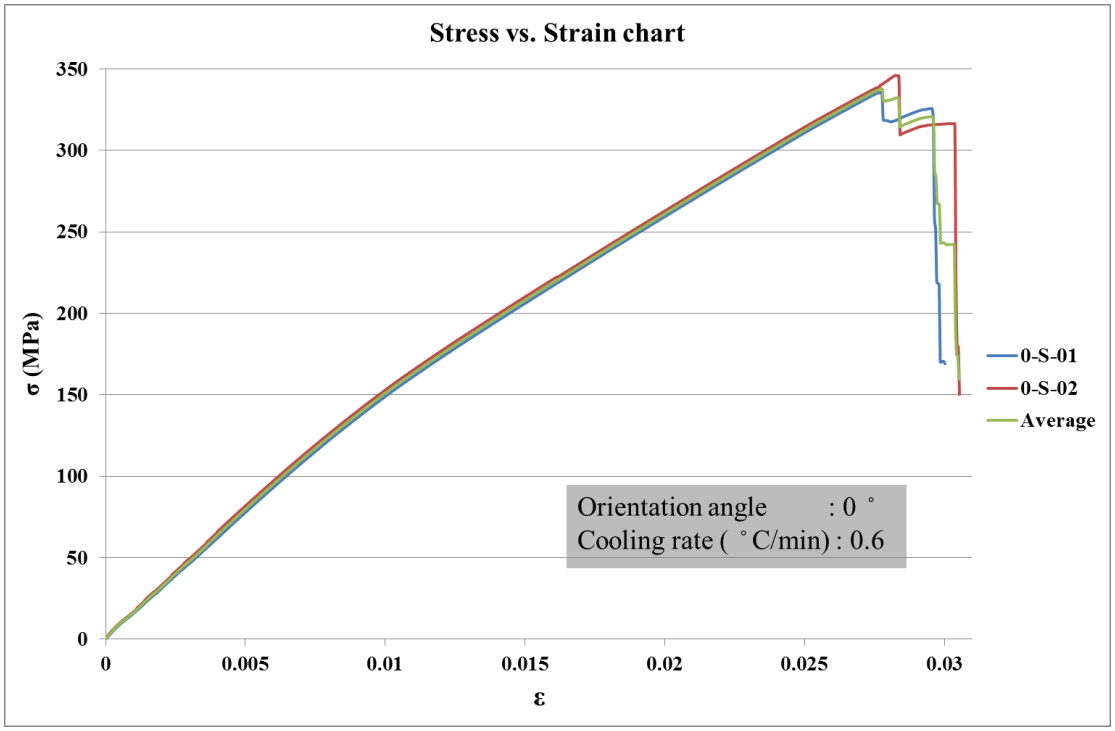

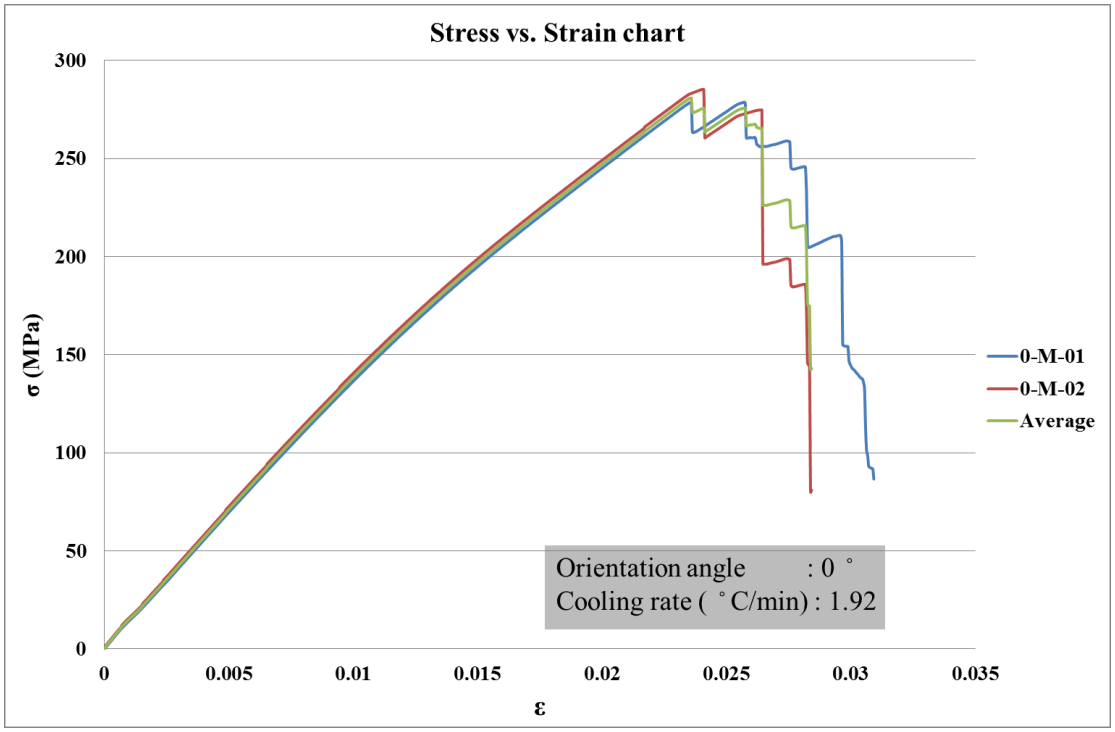

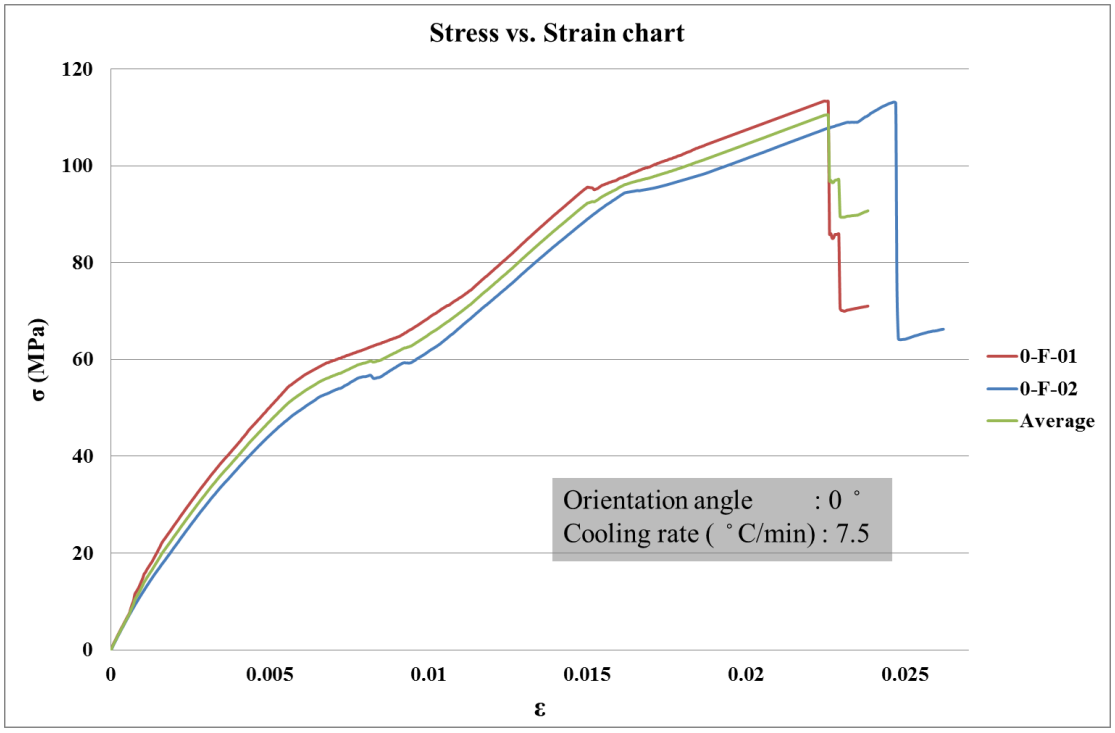
Stress vs. Strain chart
120
100
80
60
40
20
0
σ (MPa)
0
0.005
0.01
0.015
0.02
0.025
ε
Orientation angle : 0 °
Cooling rate (°C/min) : 7.5
0-F-01
0-F-02
Average

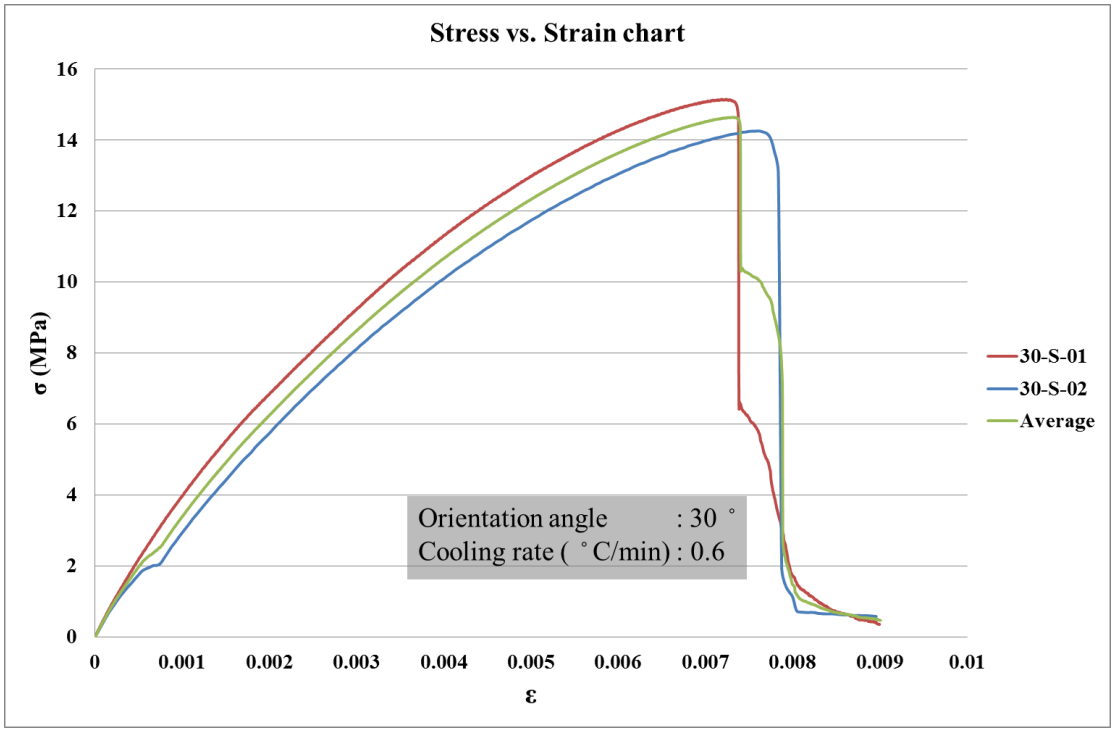
Stress vs. Strain chart
16
14
12
10
8
6
4
2
0
σ (MPa)
0
0.001
0.002
0.003
0.004
0.005
0.006
0.007
0.008
0.009
0.01
ε
Orientation angle : 30 °
Cooling rate (°C/min) : 0.6
30-S-01
30-S-02
Average

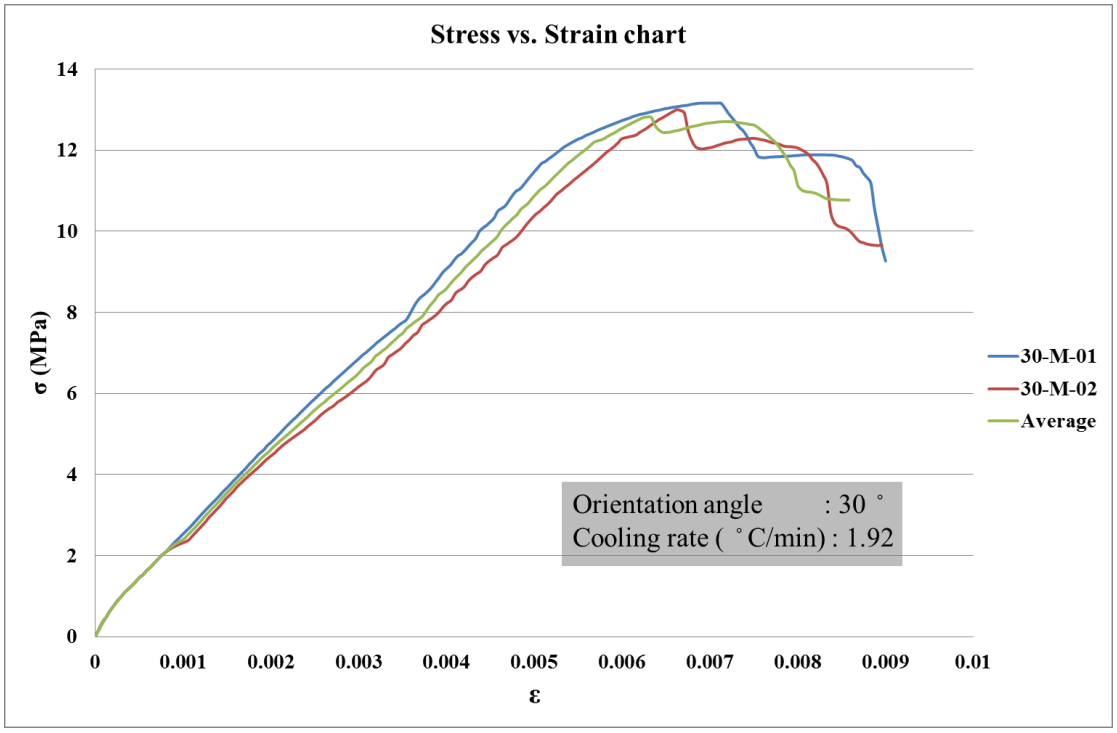
Stress vs. Strain chart
σ (MPa)
ε
0
2
4
6
8
10
12
14
0
0.001
0.002
0.003
0.004
0.005
0.006
0.007
0.008
0.009
0.01
30-M-01
30-M-02
Average
Orientation angle : 30 °
Cooling rate (°C/min) : 1.92

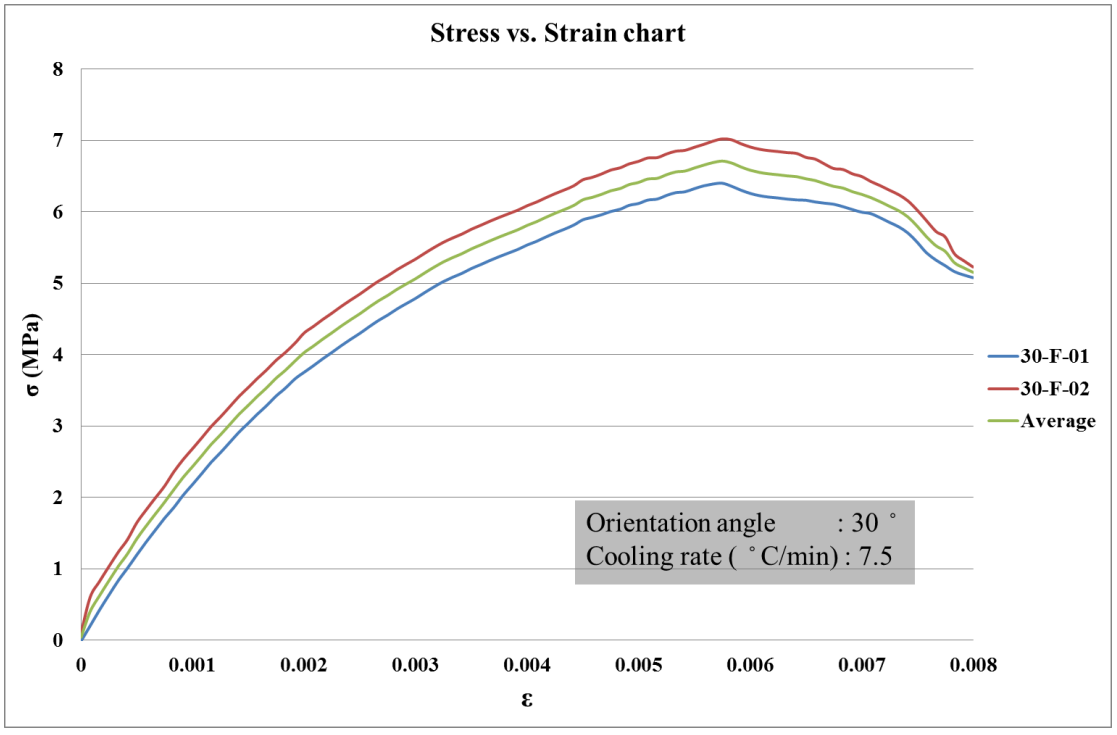
Stress vs. Strain chart
σ (MPa)
ε
0
1
2
3
4
5
6
7
8
0
0.001
0.002
0.003
0.004
0.005
0.006
0.007
0.008
30-F-01
30-F-02
Average
Orientation angle : 30 °
Cooling rate (°C/min) : 7.5

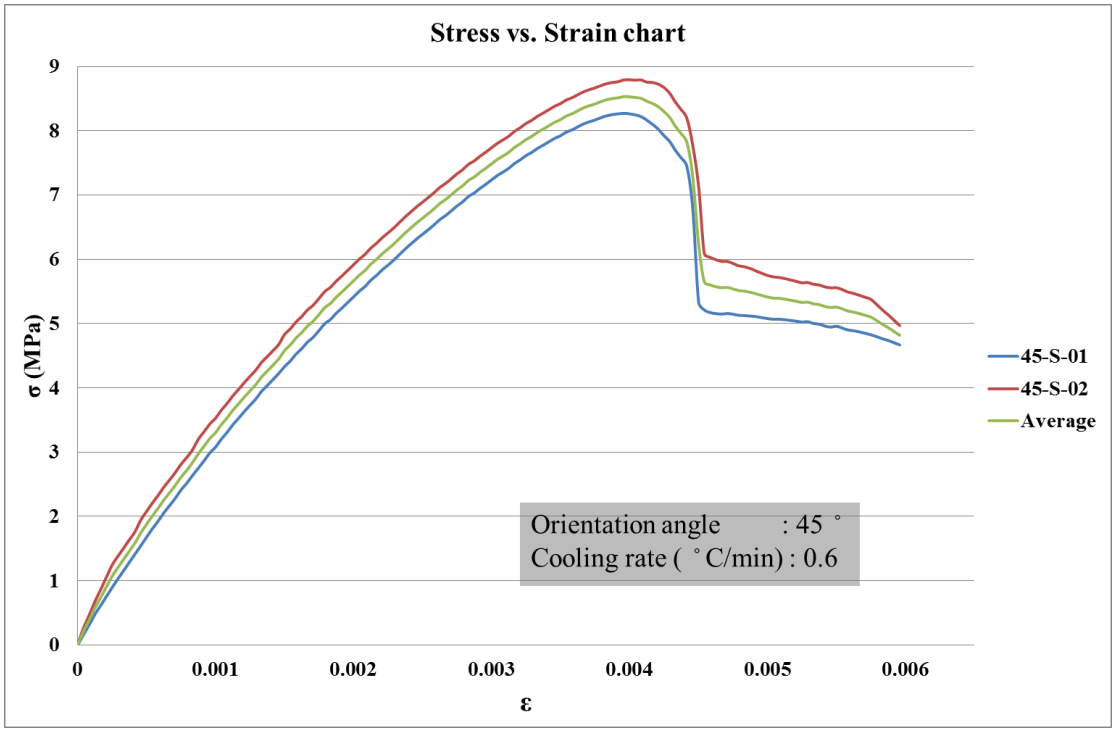
Stress vs. Strain chart
σ (MPa)
ε
0
1
2
3
4
5
6
7
8
9
0
0.001
0.002
0.003
0.004
0.005
0.006
45-S-01
45-S-02
Average
Orientation angle : 45 °
Cooling rate (°C/min) : 0.6

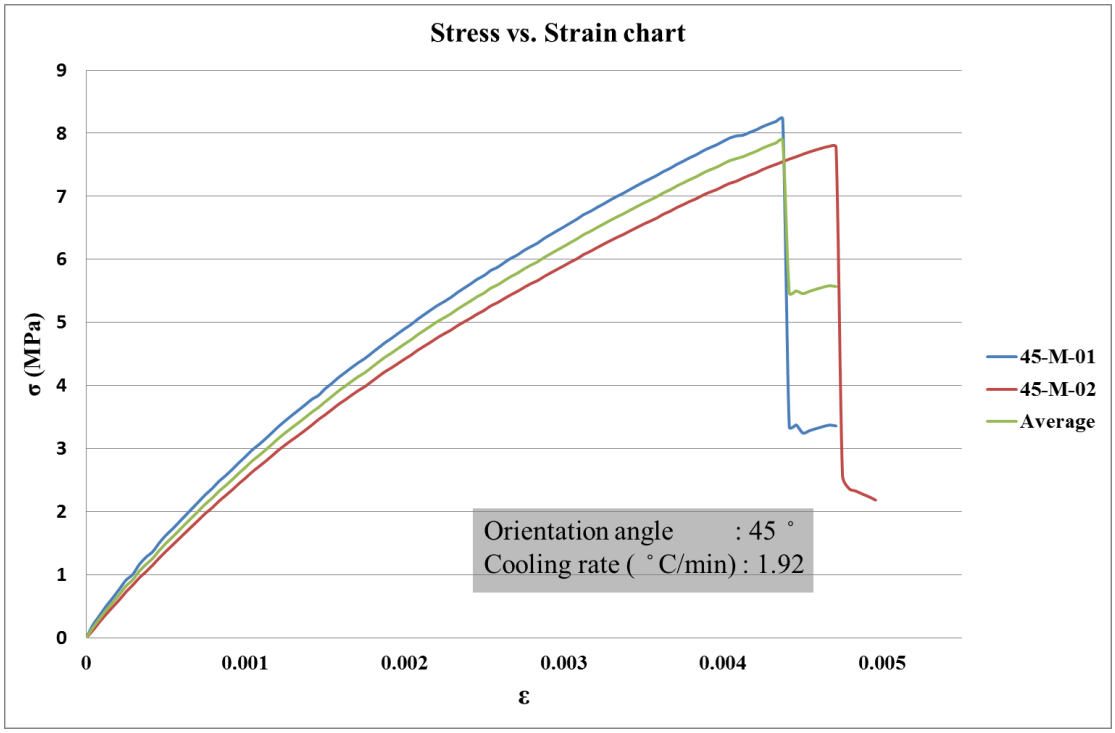
Stress vs. Strain chart
σ (MPa)
ε
0
1
2
3
4
5
6
7
8
9
0
0.001
0.002
0.003
0.004
0.005
45-M-01
45-M-02
Average
Orientation angle : 45 °
Cooling rate (°C/min) : 1.92

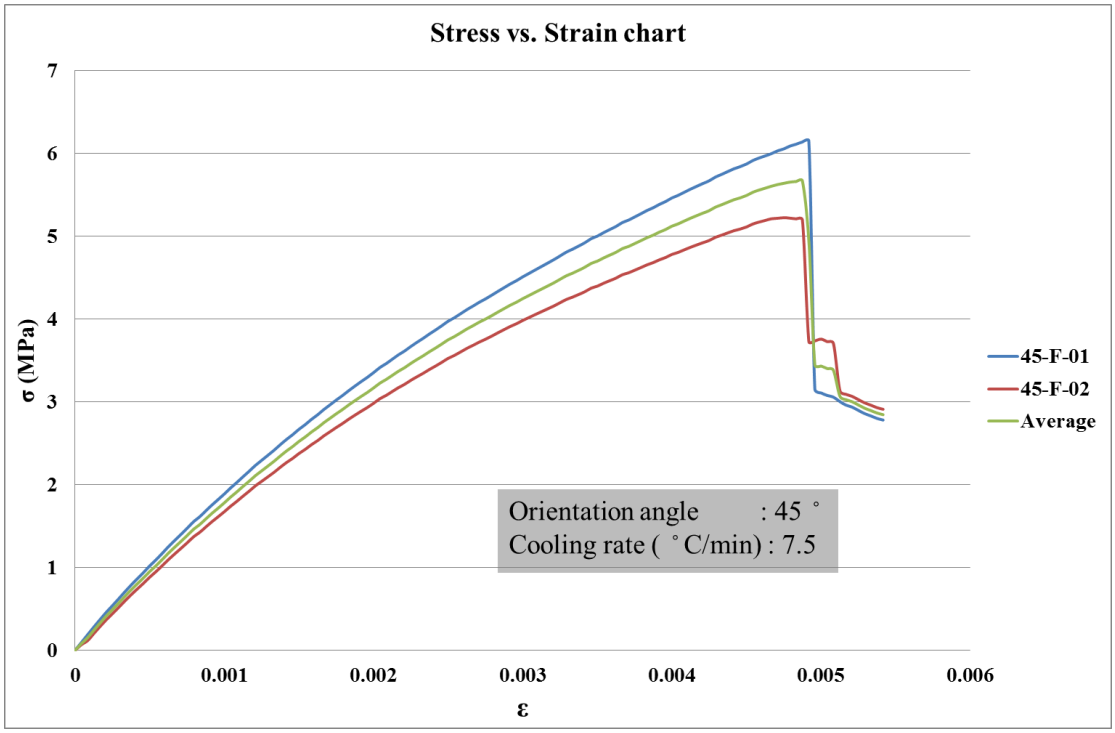
Stress vs. Strain chart
σ (MPa)
ε
0
1
2
3
4
5
6
7
0
0.001
0.002
0.003
0.004
0.005
0.006
45-F-01
45-F-02
Average
Orientation angle : 45 °
Cooling rate (°C/min) : 7.5

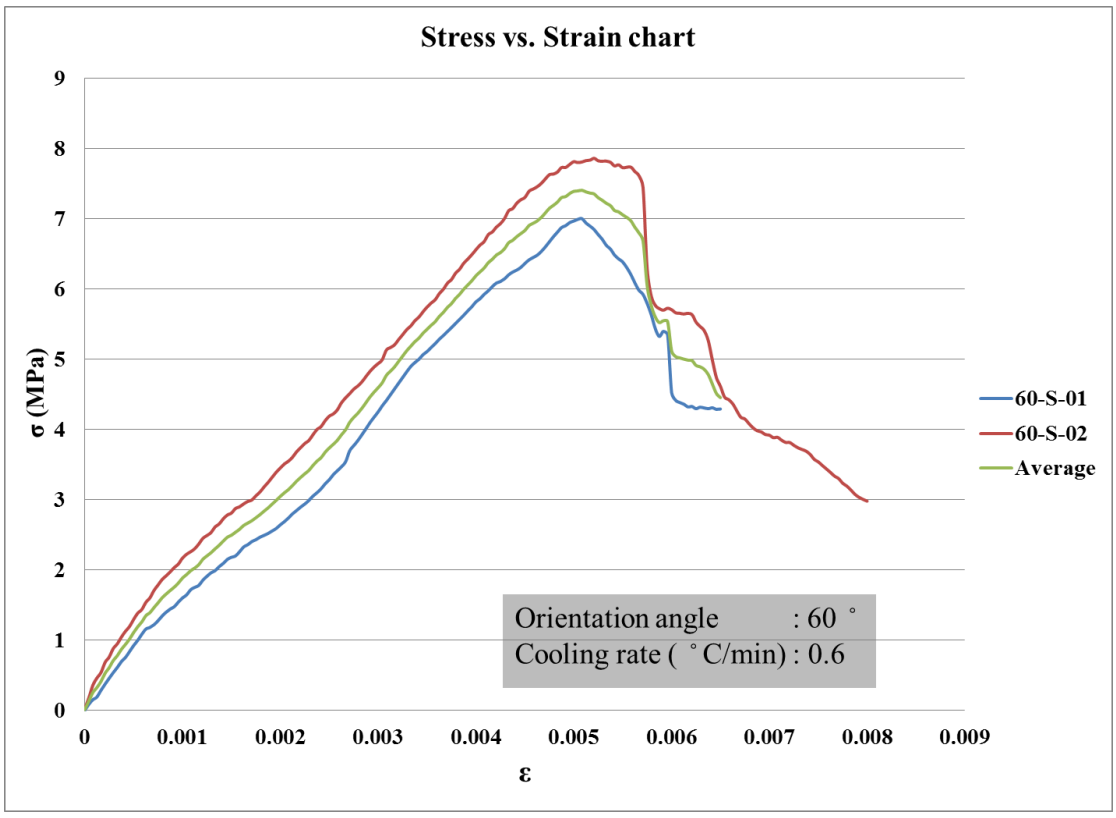
Stress vs. Strain chart
σ (MPa)
ε
0
1
2
3
4
5
6
7
8
9
0
0.001
0.002
0.003
0.004
0.005
0.006
0.007
0.008
0.009
60-S-01
60-S-02
Average
Orientation angle : 60 °
Cooling rate (°C/min) : 0.6

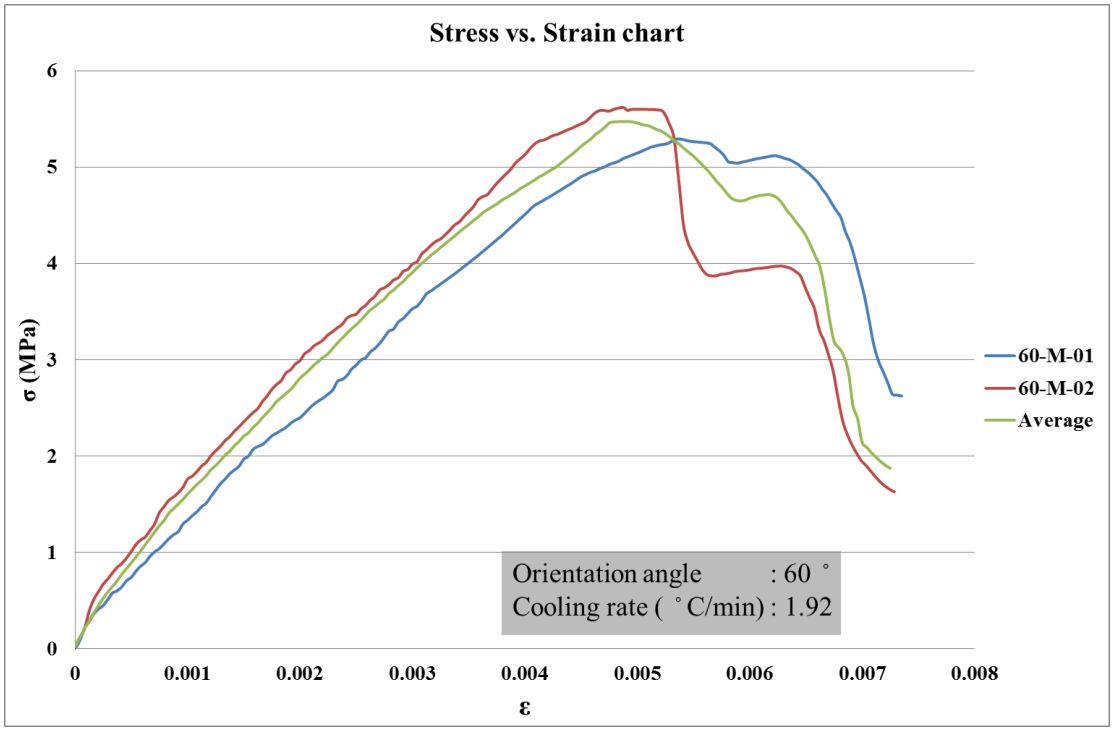
Stress vs. Strain chart
σ (MPa)
ε
0
1
2
3
4
5
6
0
0.001
0.002
0.003
0.004
0.005
0.006
0.007
0.008
60-M-01
60-M-02
Average
Orientation angle : 60 °
Cooling rate (°C/min) : 1.92

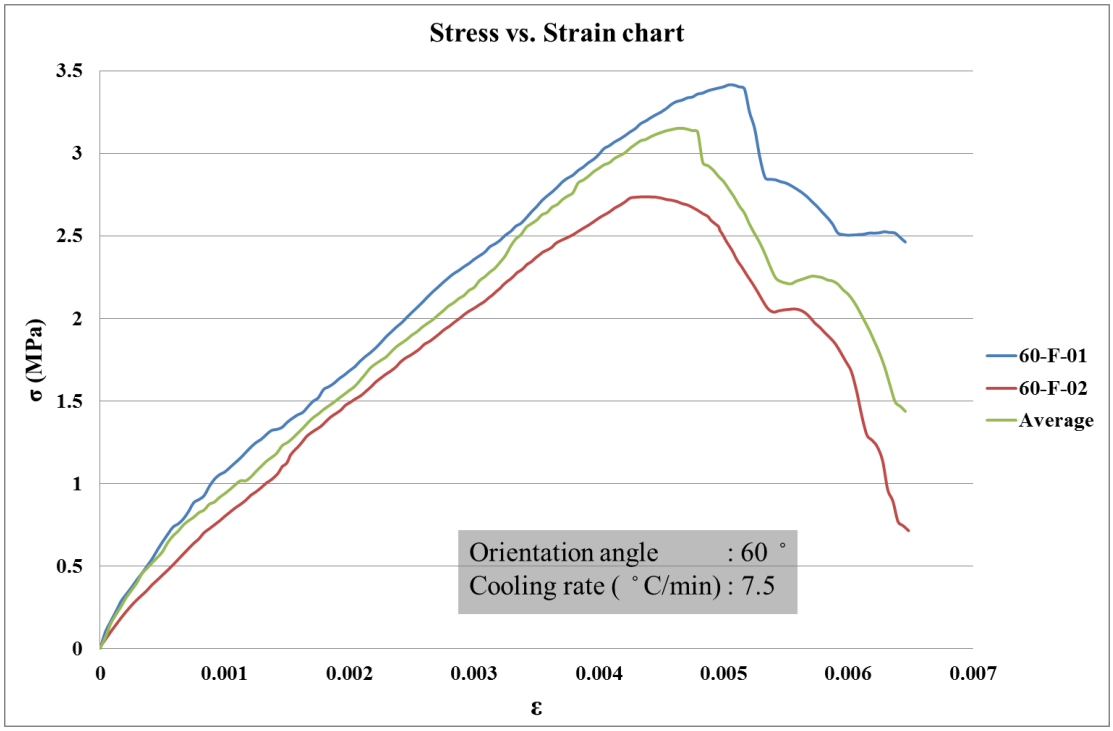
Stress vs. Strain chart
σ (MPa)
ε
0
0.5
1
1.5
2
2.5
3
3.5
0
0.001
0.002
0.003
0.004
0.005
0.006
0.007
60-F-01
60-F-02
Average
Orientation angle : 60 °
Cooling rate (°C/min) : 7.5

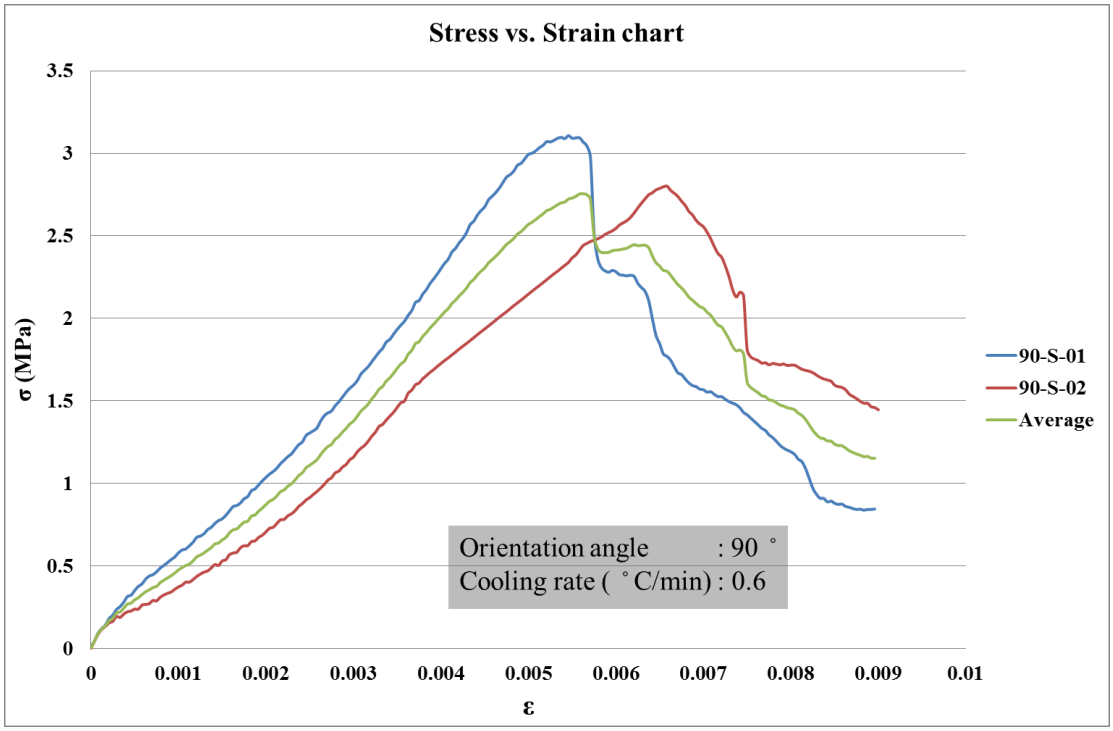
Stress vs. Strain chart
3.5
3
2.5
2
1.5
1
0.5
0
σ (MPa)
0
0.001
0.002
0.003
0.004
0.005
0.006
0.007
0.008
0.009
0.01
ε
90-S-01
90-S-02
Average
Orientation angle : 90 °
Cooling rate (°C/min) : 0.6

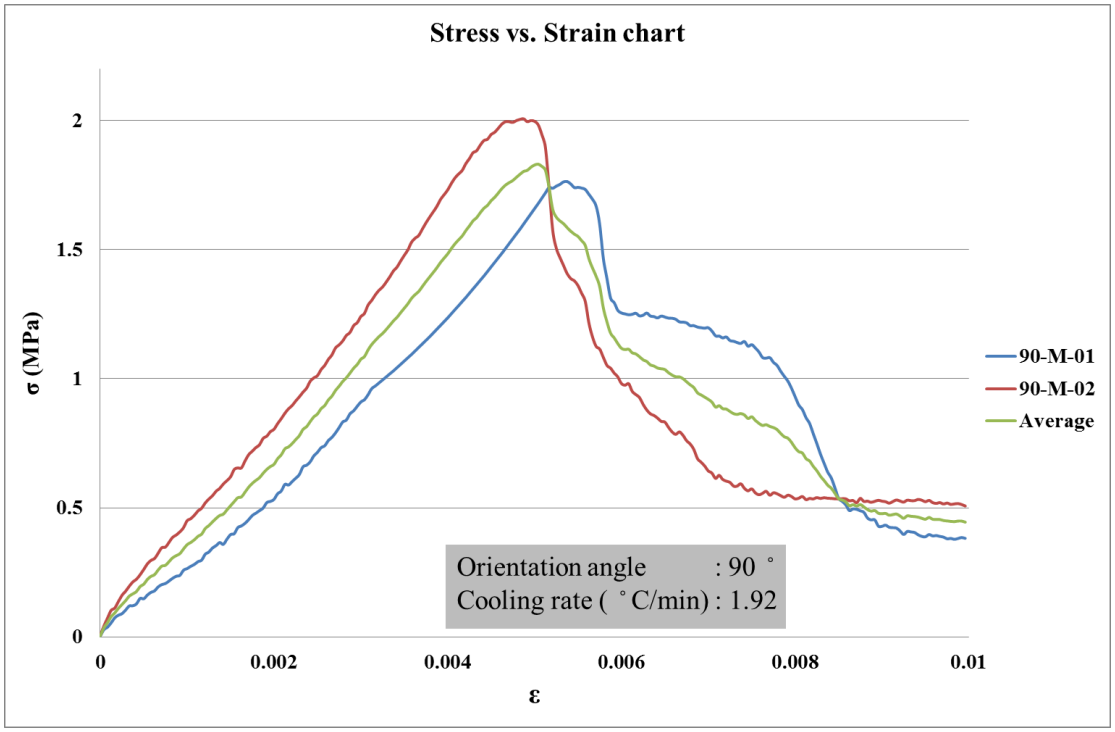
Stress vs. Strain chart
2
1.5
1
0.5
0
σ (MPa)
0
0.002
0.004
0.006
0.008
0.01
ε
90-M-01
90-M-02
Average
Orientation angle : 90 °
Cooling rate (°C/min) : 1.92

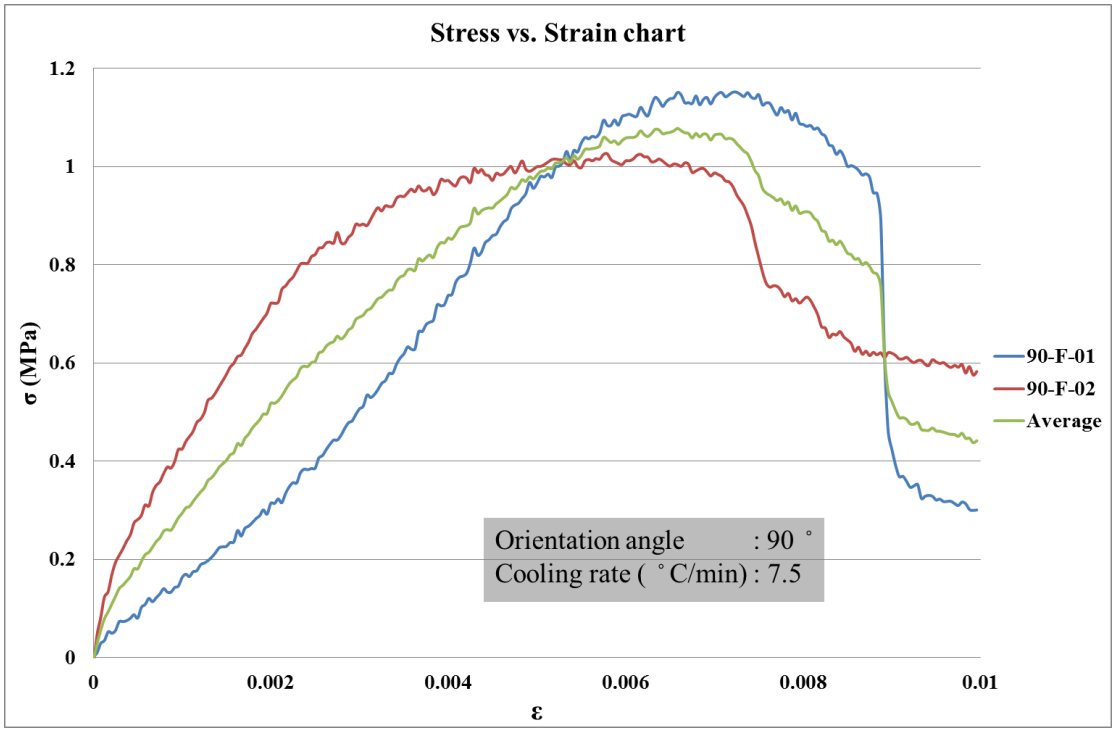
Stress vs. Strain chart
1.2
1
0.8
0.6
0.4
0.2
0
σ (MPa)
0
0.002
0.004
0.006
0.008
0.01
ε
90-F-01
90-F-02
Average
Orientation angle : 90 °
Cooling rate (°C/min) : 7.5

Vita

Mohammed Safouh Kabbani was born on March 20, 1987, in Aleppo, in Syria. He moved to UAE and got his education in local private schools and graduated from National Charity School in 2004. He received a full Scholarship to the Emirates Aviation University, Dubai, UAE, from which he graduated in 2009 with a Bachelor of Aeronautical Engineering degree.

Mr. Kabbani began a Master's program in Mechanical Engineering at the American University of Sharjah in 2009 and was enrolled in the university as a graduate teaching assistant in 2010.

Mr. Kabbani worked in various companies across the UAE. He started his professional career with Emirates Airline Engineering as production planning engineer then moved to the construction industry.

Mr. Kabbani was awarded the best engineer in Taqdeer awards 2016 and shortlisted for the MEP Middle East awards 2016 under the category young engineer of the year.